To the Graduate Council:

I am submitting herewith a thesis written by Delight Mawunyo Owu "Numerical Simulation for the Cooling of QPS Modular Coils with Embedded Copper Tubes and Subsequent Experimental Verification". I have examined the final electronic copy of this thesis for form and content and recommend that it be accepted in partial fulfillment of the requirements for the degree of Master of Science, with a major in Mechanical Engineering.

Madhu S. Madhukar

Major Professor

We have read this thesis and
recommend its acceptance:

Jay I. Frankel

Haitao Liao

Accepted for the Council:

Carolyn R. Hodges

Vice Provost and Dean of the Graduate School

(Original signatures are on file with official student records.)

Numerical Simulation for the Cooling of QPS Modular Coils with Embedded Copper Tubes and Subsequent Experimental Verification

A Thesis Presented for the
Master of Science
Degree
The University of Tennessee, Knoxville

Delight Mawunyo Owu

May 2009

DEDICATION

This thesis is dedicated to my beloved parents Mr. and Mrs. J. W. Owu, to my wife Pamela Scott Owu, and children Daja Nicole Flowers and Dwight Mawunyo Owu for their love, and support.

ACKNOWLEDGEMENTS

First and foremost, I would like to render my sincere gratitude to Dr. Madhu Madhukar, for giving me this opportunity. He has been a mentor who motivated me and was always available for assistance in the form of criticisms and suggestions which helped a lot in making this thesis successful. I would also like to thank Dr. Jay Frankel and Dr. Haitao Liao for their academic support and for serving on my thesis committee.

I am highly indebted to the people working at the Magnet Development Laboratory for their support throughout my entire master's program. I am especially thankful to the director, Robert Benson, for the financial support even during crucial times. I would like to thank Paul Goranson for his expertise that helped a lot in understanding some heat transfer concepts. I would like to give special thanks to Joe Campbell and Jim Holder for their technical expertise in preparing the conductor and experimental set-up. I would also like to thank Gary Lovett for the invaluable lessons he gave me in using the Pro-Engineer software.

To my friend, Ernest Kwaku Kraka, I seize this opportunity to say a big "thank you" for making time to proof-read this work. I am very grateful for the suggestions you gave that made this work successful.

Last but not least, I would like to thank my wife's parents, Mr. and Mrs. Johnny Davis, for their love, care, and support throughout my entire master's program.

ABSTRACT

Quasi Poloidal Stellarator (QPS) consists of complex shaped modular coils, made of Copper-CTD 403 cyanate ester composite, that are used to carry the heavy current (~30,000 amperes) for the plasma generation. The coils become heated during each plasma pulse from 20°C to about 60°C. The coils need to be cooled back to room temperature after each pulse in order to prevent temperature ratcheting over the duty cycle. After studying various approaches, it was found that the most efficient way of cooling was by passing water through a copper tube embedded inside every conductor. Previously developed numerical approach based on the lumped analysis assumed constant temperature within the copper and the water lumps. Also, the axial conduction along the conductor length was neglected. Considering the large conductivity in the axial direction, 320 W/(mK), compared to that in the radial direction, 9.9 W/(mK), the neglect of axial conduction could be an oversimplification of the problem.

The aim of this thesis was to modify the lumped model to include the axial heat conduction in addition to the radial heat conduction and to compare the predictions with experimentally recorded cooling data on 5.5 m and 12.2 m long conductors when they were heated to 60°C and 80°C and cooled with water at different flow rates. The conductor was fabricated using the vacuum pressure impregnation technique. The results from the model showed that although the conductivity in the axial direction was much larger than that in the radial direction, almost all the heat transfer was in the radial direction. The agreement between the model predictions and the experimental data on 12.2 m long conductor was poor, especially at points away from the conductor inlet. The reasons for this poor agreement were attributed to a variety of heat transfer mechanisms that existed in the actual experiments but were not accounted for in the model. Additional modeling work needs to be conducted before the validity of the model for predicting the cooling behavior of long conductors can be determined.

List of Symbols / Abbreviations

Symbols

A	area under the temperature profile for initial time
A_1	area under the temperature profile of from x=0 to x=L/2 for small times
A_2	half of the area under the temperature profile for initial time
A_3	area under the temperature profile from x=L/2 to x=L for small times
ΔA_1	proportional heat loss area by middle conductor element to element 1
ΔA_3	proportional heat gain area by middle conductor element from element 3
Bi	Biot number
C_{pcomp}	specific heat capacity of the composite, J/(kgK)
C_{pwater}	specific heat capacity of water, J/(kgK)
D	inside diameter of pipe, m
f	pipe friction factor
Fo	Fourier modulus
g	acceleration due to gravity, m/s^2
h	convective heat transfer coefficient, $W/(m^2K)$
k_r	thermal conductivity of composite in the radial direction, W/(mK)
k_x	thermal conductivity of composite in the axial direction, W/(mK)
L	length of an element of the conductor, m
L_c	length of conductor, m
L^*	radial heat resistance parameter
m_{comp}	mass of a composite element, kg
m_{water}	mass of a water element, kg
Pr	Prandtl number
Δp	pressure drop, N/m^2
Re	Reynolds number
t	time step, s
T_{fcomp}	final temperature of composite element after interacting with water, °C
T_{fcomp1}	final temperature of composite element 1 after radial conduction, °C

T_{fcomp2}	final temperature of composite element 2 after radial conduction, °C
T_{fcomp3}	final temperature of composite element 3 after radial conduction, °C
T_{fwater}	final temperature of water, °C
T_{icomp}	initial temperature of composite, °C
T_{iwater}	initial temperature of water, °C
$T_{upcomp1}$	updated temperature of element 1 after axial conduction, °C
$T_{upcomp2}$	updated temperature of element 2 after axial conduction, °C
$T_{upcomp3}$	updated temperature of element 3 after axial conduction, °C
v	velocity of flow, m/s

Greek letters

α	thermal diffusivity, m^2/s
ρ	density, kg/m^3
θ	dimensionless temperature
λ	eigenvalues

Abbreviations

AWE	Asymptotic Waveform Evaluation
CTD	Composite Technology Development, Inc.
LMAC	Lumped Model with axial conduction between conductor elements
MATLAB	Matrix Laboratory
NPT	National Parts Thread
ORNL	Oak Ridge National Laboratory
QPS	Quasi-Poloidal Stellarator

TABLE OF CONTENTS

1. INTRODUCTION 1
   1.1 Overview 1
   1.2 Tokamak 3
   1.3 Stellarator 3
      1.3.1 Quasi Poloidal Stellarator (QPS) 3
   1.4 Scope of the Study 5
2. LITERATURE REVIEW 7
   2.1 Research Studies 7
3. MATERIALS AND METHODS 12
   3.1 Conductor 12
   3.1.1 Ground wrap/insulation: 13
   3.1.2 Winding of conductor: 14
   3.1.3 Vacuum Impregnation: 15
   3.1.4 Heating and Curing: 16
   3.2 Experimental Setup 18
   3.3 Experimental Procedure: 19
      3.3.1 Heating Process: 21
      3.3.2 Cooling Process: 21
4. NUMERICAL SIMULATION 24
   4.1 Elemental Model 24
   4.2 Radial conduction analysis 25
   4.3 Axial conduction analysis 26
5. RESULTS AND DISCUSSIONS 37
   5.1 Overview 37
   5.1.1 Investigating the effect of axial conduction on the lumped model 37
   5.1.2 Comparison between Experimental and LMAC Results 43
6. CONCLUSIONS 56
7. FUTURE WORK 58
REFERENCES 59
APPENDICES 63
   Appendix A 64
   Appendix B 70
VITA 76

LIST OF TABLES

Table **Page**

4.1 Properties of the conductor used in the lumped model. 36

LIST OF FIGURES

Figure **Page**

1.1 World Marketed Energy Consumption from 1980 to 2030 [2]. 1
1.2 Fusion of deuterium and tritium to release energy [6]. 2
1.3 A cut-away view of the QPS. 4
1.4 Various cooling concepts with Option I as the most efficient [10]. 5

3.1 Enlarged cross-sectional view of the conductor. 12
3.2 Steel winding form with insulation applied. 13
3.3 Conductor wound on the winding form. 14
3.4 Vacuum Impregnation System. Conductor is mounted on oven 15
3.5 Curing cycle used for the polymer. 16
3.6 Pie arrangement of 12.2 m conductor sets for experiment. Pie 1 is closest. 17
3.7 Experimental setup used for the experiment. 18
3.8 Enlarged view of the experimental setup showing individual components. 1) Main water valve; 2) Pressure gauge; 3) Data logger; 4) Oven controller; 5) Forced air convention oven; 6) Flow meters; 7) Hose; 8) Pump. 19
3.9 Conductor mounted on oven door (A), Conductor on oven door covered with insulation blanket (B), and Conductor pushed inside oven and door secured with C-clamps. All exposed tubes are covered with insulation material (C). 20
3.10 A typical experimental results obtained when the conductor was heated to 60.2°C and cooled with water flowing at a rate of 0.1 GPM. The 'heating cycle' refers to the complete heating period, the 'wait period' being the time when the oven elements were allowed to cool down and temperatures allowed to stabilize, and the 'cooling cycle' refers to the duration of cooling by introducing water into the conductor. 23

4.1 Elemental model. The direction of heat flow is shown by solid arrows. 25
4.2 Three composite elements. 27
4.3 Representation of the problems. (a) description of the problem using equations 4.3, (b) description of the problem using equations 4.8 28
4. 4 Typical temperature profile of the middle element for various times during the interaction with neighboring elements: (a) time = 0; (b) time = 0.01 sec.; (c) time = 1 sec. 33

5.1 Comparisons between experimental and predicted cooling curves (at locations of 4.5%, 25%, 75%, and 95% of the conductor length) for lumped model and lumped model with axial conduction when a 5.5m long conductor was cooled by 18°C water flowing through the cooling tube at 0.1GPM. In all predictions, the heat resistance parameter, L*, was 9 mm. 38

Figure **Page**

5.2 Comparisons between experimental and predicted cooling curves (at the supply, middle, and return of the conductor length) for lumped model and lumped model with axial conduction when 12.2m long conductor was cooled by 9.9°C water flowing through the cooling tube at 0.1GPM. In all predictions, the heat resistance parameter, L*, was 9mm. 39
5.3 Comparisons between predicted cooling curves (at locations of 25%, 55%, and 95% of the conductor length) for lumped model and lumped model with axial conduction when a 5.5m long conductor was cooled by 18°C water flowing through the cooling tube at 0.1GPM. In all predictions, the heat resistance parameter, L*, was 9 mm. 41
5.4 Magnified view of Figure 5.3 to clearly show the comparisons between predicted cooling curves (at locations of 25%, and 55% of the conductor length) for lumped model and lumped model with axial conduction when a 5.5m long conductor was cooled by 18°C water flowing through the cooling tube at 0.1GPM. In all predictions, L* was 9 mm. 42
5.5 Comparisons between experimental and predicted cooling curves (at the supply, middle, and return of the conductor length) for lumped model and lumped model with axial conduction when 12.2m long conductor was cooled by 9.9°C water flowing through the through the cooling tube at 0.1GPM. In all predictions, the heat resistance parameter, L*, was 9 mm. 44
5.6 Comparisons between experimental and predicted cooling curves (at the supply, middle, and return of the conductor length) for the lumped model with axial conduction when a 12.2m long conductor was cooled by 9.8°C water flowing through the cooling tube at 0.15 GPM. In all predictions, the heat resistance parameter, L*, was 9 mm. 45
5.7 Comparisons between experimental and predicted cooling curves (at the supply, middle, and return of the conductor length) for the lumped model with axial conduction when a 12.2m long conductor was cooled by 9.1°C water flowing through the cooling tube at 0.2 GPM. In all predictions, the heat resistance parameter, L*, was 9 mm. 46
5.8 Comparisons between experimental and predicted cooling curves (at the supply, middle, and return of the conductor length) for the lumped model with axial conduction when a 12.2m long conductor was cooled by 9.4°C water flowing through the cooling tube at 0.25 GPM. In all predictions, the heat resistance parameter, L*, was 9 mm. 47
5.9 Comparisons between experimental and predicted cooling curves (at the supply, middle, and return of the conductor length) for the lumped model with axial conduction when a 12.2m long conductor was cooled by 9.5°C water flowing through the cooling tube at 0.3 GPM. In all predictions, the heat resistance parameter, L*, was 9 mm. 48

Figure **Page**

5.10 Comparisons between experimental and predicted cooling curves (at the supply, middle, and return of the conductor length) for the lumped model with axial conduction when a 12.2m long conductor was cooled by 10°C water flowing through the cooling tube at 0.1 GPM. In all predictions, the heat resistance parameter, L*, was 9 mm. 49
5.11 Comparisons between experimental and predicted cooling curves (at the supply, middle, and return of the conductor length) for the lumped model with axial conduction when a 12.2m long conductor was cooled by 9.8°C water flowing through the cooling tube at 0.15 GPM. In all predictions, the heat resistance parameter, L*, was 9 mm. 50
5.12 Comparisons between experimental and predicted cooling curves (at the supply, middle, and return of the conductor length) for the lumped model with axial conduction when a 12.2m long conductor was cooled by 10°C water flowing through the cooling tube at 0.2 GPM. In all predictions, the heat resistance parameter, L*, was 9 mm. 51
5.13 Comparisons between experimental and predicted cooling curves (at the supply, middle, and return of the conductor length) for the lumped model with axial conduction when a 12.2m long conductor was cooled by 10.3°C water flowing through the cooling tube at 0.25 GPM. In all predictions, the heat resistance parameter, L*, was 9 mm. 52
5.14 Comparisons between experimental and predicted cooling curves (at the supply, middle, and return of the conductor length) for the lumped model with axial conduction when a 12.2m long conductor was cooled by 9.6°C water flowing through the cooling tube at 0.3 GPM. In all predictions, the heat resistance parameter, L*, was 9 mm. 53
5.15 A section of conductor winding showing the possibility of heat transfer between adjacent layers. 55

1. INTRODUCTION

1.1 Overview

Approximately 80% of the world's energy comes from non-renewable fossil fuels which when combusted release greenhouse gases into the atmosphere. Fossil fuels- coal, oil, and natural gas were formed hundreds of millions of years ago. These energy sources are becoming scarce due to a steady increase in their consumption worldwide [1]. According to the Energy Information Administration projection [2], the world energy consumption will increase by 50 percent from 2005 to 2030, as shown in Figure 1.1.

Increasing concern about the long-term availability of fossil fuels, greenhouse gas emissions, and energy security, has led to increased interest in the use of renewable sources such as wind, solar, biomass, geothermal, and nuclear. Some people are proposing that nuclear power will provide clean, low-carbon, electricity for many generations to come [3].

Nuclear power was originally developed in the 1950s for the peaceful application of the large quantities of energy released by the splitting of atoms, or "nuclear fission," and by 2001 it accounted for 17% of all electricity produced worldwide. It provides a significant share of electrical power generation in some countries. For example, nuclear energy accounts for nearly 80% of all electrical power production in France [1].

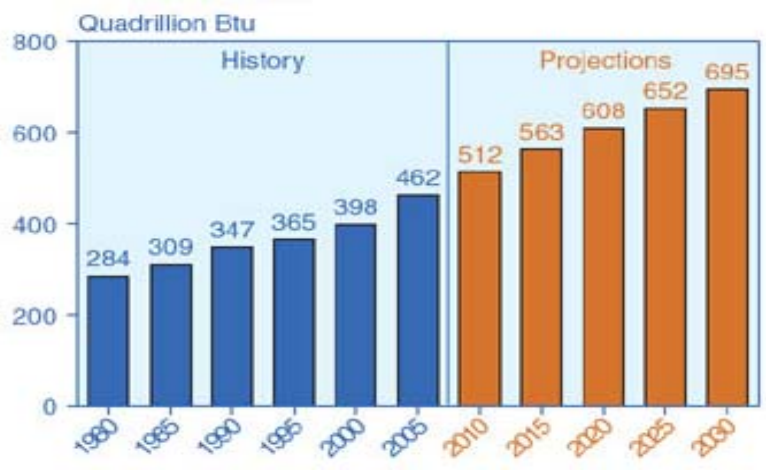

Figure 1.1 World Marketed Energy Consumption from 1980 to 2030 [2].

Although nuclear energy is generated either through atomic fission or fusion, all nuclear power plants operating currently rely on fission. However, the biological hazards associated with nuclear fission make it an unpopular option for the energy needs of the future. Wastes generated from nuclear fission remain radioactive for several thousands of years [4].

Nuclear fusion- the process which powers the sun may be the solution to energy needs of the future. The most common fusion reaction that is being researched for energy generation is the fusion of deuterium atom with tritium atom, both isotopes of hydrogen. Both of these isotopes are abundant on earth. Deuterium can be extracted from ordinary seawater, and tritium can be bred from lithium. The energy potential for fusion energy is enough to supply the world with energy for at least 5,000 years [5]. In the fusion reaction, deuterium and tritium atoms fuse together to produce helium and a large amount of energy is released during this process [6], as shown in Figure 1.2.

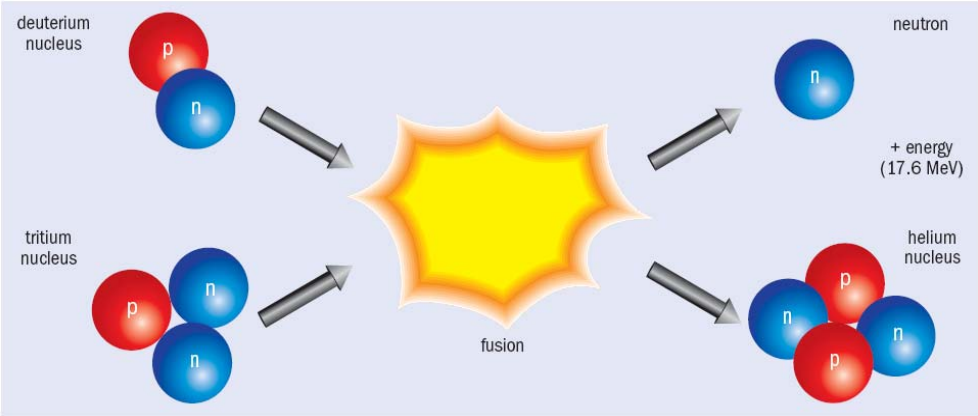

Figure 1.2 Fusion of deuterium and tritium to release energy [6].

It is obvious that controlled fusion has fewer negative aspects than fission. There are no serious long term spent-fuel reprocessing or waste problems and there is no potential for the large scale release of radioactivity. However, the controlled fusion reaction has two major challenges 1) heating the fuel to temperatures of about 100 million degrees Celsius needed for fusion to occur. The ideas that are being tried to heat the plasma are ohmic heating, ion beam heating, and radio wave heating, and 2) containment of the hot plasma since there is no single material that can withstand such temperatures. There are two types of vessel design, both based on magnetic confinement are being tried - the tokamak or torus and the stellarator [5].

1.2 Tokamak

The tokamak is a doughnut-shaped chamber in which plasma is heated by means of inducing current in plasma, ion beam heating and radio wave heating. The plasma is confined by magnetic fields by means of a series of coils [7, 8]. Since the research presented in this thesis related to the stellarator type of vessel, we present a more detailed description of stellarators.

1.3 Stellarator

The stellarator is a device used to confine hot plasma in magnetic fields that are generated entirely by external coils, i.e. there is no plasma current induced. Researchers have shown that stellarators achieve distinctly higher plasma densities and do not suffer from plasma disruptions like in tokamaks [6]. An example of this device is the Quasi-Poloidal Stellarator (QPS).

1.3.1 Quasi Poloidal Stellarator (QPS)

Quasi-Poloidal Stellarator (QPS) is a low-aspect ratio, concept exploration experiment with a non-axisymmetric, near-poloidally-symmetric magnetic configuration. This project is currently in its early design phase and is being investigated jointly by ORNL and the University of Tennessee [9]. A cut-away view of the stellarator is shown in Figure 1.3.

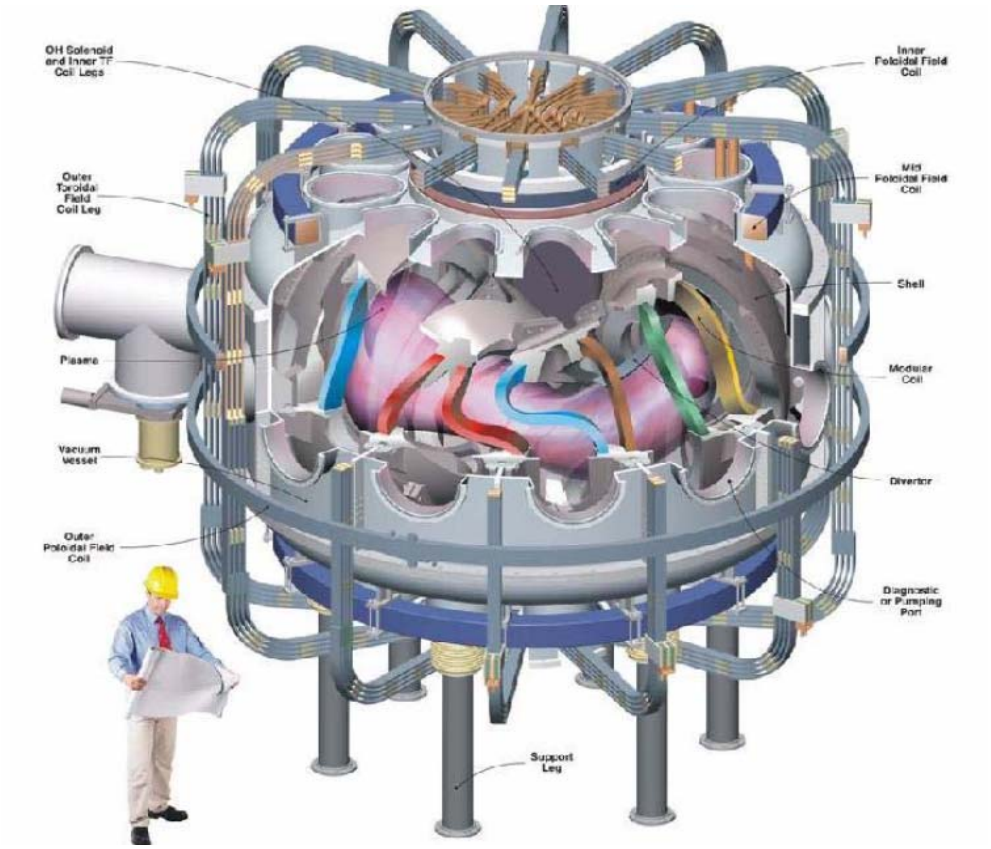

Figure 1.3 A scaled cut-away view of the QPS.

QPS consists of complex shaped modular coils, made of Copper- CTD 403 cyanate ester composite, that are used to carry the heavy current (~30,000 amperes) needed to generate the plasma. During each pulse of plasma generation, the coils become heated from room temperature (20°C) to about 60°C. In order to prevent temperature ratcheting over the duty cycle, the coil needs to be cooled back to room temperature after each pulse of plasma generation. Freudenberg et al. [10] studied various approaches for cooling the modular coils and found that the most efficient way of cooling the coil was by embedding a copper tube inside every conductor and passing water through. This is shown in option I of Figure 1.4.

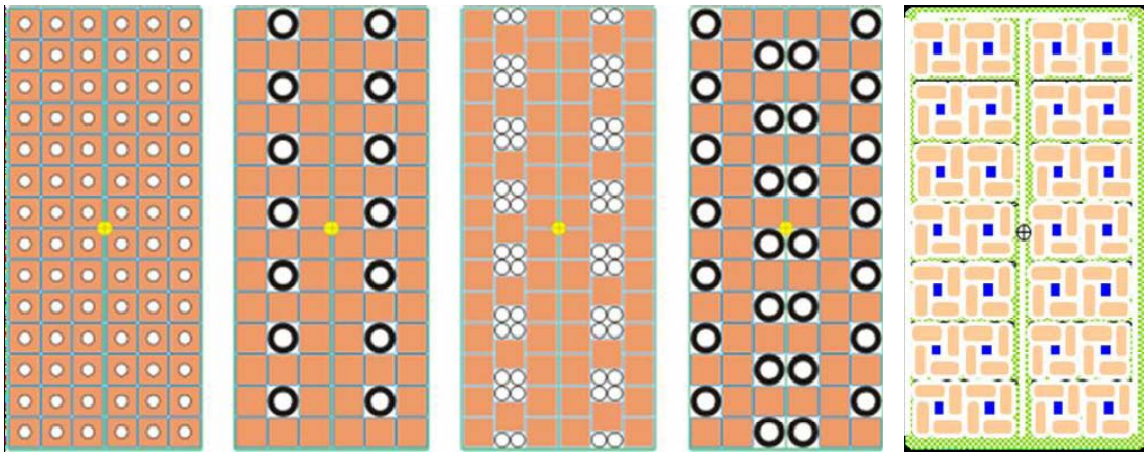

Option I
Each conductor has a cooling tube embedded

Option II
Columns of flexible Teflon tubing

Option III
Groups of small copper tubing

Option IV
Staggered array of flexible tubing

Option V
Conductor with square cooling

Figure 1.4 Various cooling concepts with Option I as the most efficient [10].

Using the proposed cooling method, past research has been done on some relatively short conductors to predict their cooling behavior, i.e. the rate of change of temperature at different points along its length as a function of time (dT/dt). However, no research has been done for long coils and that is the focus of this thesis.

1.4 Scope of the Study

Past research that used a radially lumped analysis to investigate the cooling behavior of QPS modular coils focused on only heat transfer due to radial conduction of the coil [11,12]. The effect of axial conduction along the length of the conductor was neglected. However, considering the large conductivity in the axial direction, 320 W/(mK), compared to that in the radial direction, 9.9 W/(mK), this could be an oversimplification of the problem since heat would be conducted both in the radial and axial directions of the composite. The purpose of this thesis is to investigate the cooling behavior of a 40 ft long conductor taking into account both radial and axial directions of heat transfer. Initial plan was to investigate the cooling of both 40-ft and 80-ft long conductors. However, due to problems encountered during the vacuum pressure impregnation (VPI) of the 80-ft long conductor, only the 40-ft long conductor was investigated. A computational analysis

is made in MATLAB-7 and the predicted results were compared with experiments on the 40-ft long conductor.

2. LITERATURE REVIEW

2.1 Research Studies

In this thesis, a long conductor is considered as an n-element composite media whose elements interact with each other through axial conduction. While several studies have been published on transient heat transfer analysis in composite material, research on transient heat transfer analysis in long conductors is scarce. This section provides an overview of previous studies that are relevant to this thesis.

Sun and Wichman [13] derived a theoretical solution of a one-dimensional transient heat conduction problem in a three-layer composite slab. The eigenfunction expansion technique was used to derive a series solution for impulse heating. When the solution was compared with a finite difference numerical solution, the eigenfunction method provided an easily calculated exact solution that required only a few terms even for large times. It also had the advantage of handling cases where one layer had vastly different thermo physical properties from the other two layers, or where one layer was much narrower than the other two. In such cases, a transformation of coordinates was necessary before the finite difference numerical solution will be accurate.

Salt [14] studied the response of a two-dimensional multi-layer composite conducting slab to sudden changes in the temperature of a surrounding fluid. A general solution for the temperature profile was developed for any multi-layer two-dimensional slab whose layers are in perfect thermal contact. It was in the form of a two-dimensional coupled infinite series with exponential time decay. It was also shown that this derived solution reduced to the well-known form for the homogeneous slab. In the case of three- and two-layer slabs, the solutions were given in algebraic form suitable for desk calculations with a programmable calculator.

Monte [15] analyzed the response of one-dimensional multilayered composite conducting slab to sudden variations in the temperature of the surrounding fluid. A complete series solution was obtained by applying the method of separation of variables to the heat

conduction equation. This solution completely described the thermal field in any one of the layers and allowed for determination of the amount of heat exchanged between the composite slab and surrounding fluid. Dimensionless variables and groups were also introduced to simplify the solution to the transient two-layer problem.

Chopra and Marwah [16] studied transient heat transfer in composite media with non-linear radiation boundary condition using implicit finite difference scheme. The temperature profile was found for both regions of a composite solid consisting of two infinitely extending plates. It was observed that as the time increased, the heat transfer to the non-radiating region increased and as the diffusivity ratio decreased there was more heat transfer from the radiating surface towards the non-radiating surface.

Bilir and Ates [17] investigated transient conjugated heat transfer for laminar flow in the thermal entrance region of thick walled pipes. The problem was handled for an initially isothermal, infinitely long, thick-walled and two-regional pipe for which the upstream region was insulated and solved numerically by a finite difference method for hydro dynamically developed flow with a step change in the ambient fluid temperature in the heated downstream region. A parametric study was done to analyze the effects of five defining parameters namely, wall thickness ratio, wall-to-fluid conductivity ratio, wall-to-fluid thermal diffusivity ratio, the Peclet number and the Biot number. It was found that the effects of wall conjugation and fluid axial conduction on heat transfer characteristics increased with increasing wall thickness ratio, and decreasing wall-to-fluid thermal conductivity ratio, wall-to-fluid thermal diffusivity ratio, the Peclet number, and the Biot number. It was also found that changes in the parameter values affected the time to reach steady state and for each parameter the time increased with increasing effect.

Loh et al. [18] used asymptotic waveform evaluation (AWE) for fast transient characterization of Fourier and non-Fourier heat conduction. The Fourier and non-Fourier equations were reduced to a system of linear differential equations, respectively, using finite element method and then solved with AWE. It was found that AWE provided an

equivalent accuracy in its solution and was at least three orders faster in terms of computational time as compared to conventional iterative solvers. It was also found that the accuracy was independent of the time step used and it had the capability of providing local transient solution.

Corlay and Advani [19] studied the temperature distribution in a thin composite plate exposed to a concentrated heat source. Two heat sources were used in the experiment- a radiant heater and a gas burner flame. Varying parameters such as material properties, geometry, heat flux and distance, the temperature distribution was measured with an infra-red camera. After that, a finite element method based software, Wintherm, was used to predict the temperature distribution. The numerical results were found to be in good agreement with the experimental results. However, the prediction was more accurate for a lower heat source.

Yi et al. [20] investigated the transient coupled heat transfer in an anisotropic scattering two-layer composite slab with semitransparent surfaces. Specular reflection was considered and reflectivities were determined by Fresnel's law and Snell's law. A fully implicit control-volume method was used to solve the transient energy equation while a ray-tracing/nodal-analyzing method was used to compute the radiative information. The results showed that in a semitransparent medium with natural surfaces, two types of temperature peaks appear in transient heat transfer. One is caused by external radiation heating and environmental convection cooling, existing in steady state too. The other is due to maximum of absorption of heat caused by inhomogeneous optical properties, only existing in transients of heat transfer.

Haji-Sheikh et al. [21] examined the steady state conduction of heat from a wall to a fluid moving at a uniform velocity. The wall was heated by step changes in temperature. The mathematical procedure led to computation of the temperature field and heat transfer coefficient. In the presence of a step change in the wall temperature, it was shown that the Stanton number was a function of only the Peclet number. It was also shown that near the

thermal entrance location, heat conduction dominates and the local heat flux becomes independent of velocity. This phenomenon applied to classical convection problems in various-shaped ducts.

Beck et al. [22] investigated conduction in rectangular plates with boundary temperatures specified. It was observed that steady-state components of heat conduction solutions have very slowly convergent series for temperatures and non-convergent heat fluxes for temperature boundary conditions. To solve this problem, it was suggested that the poorly-convergent or non-convergent series be replaced by closed-form algebraic solutions.

Gordeliy et al. [23] developed a semi-analytical solution for a transient heat conduction problem for an infinite medium containing two non-overlapping circular cavities. For each cavity, the Laplace transform method was used to get Fourier series solutions for the temperatures. The addition theorem was applied to get one complete series solution of basis functions and after proper truncation of the series solution, inversion of the Laplace transform was performed to bring the solution back to the space-time domain. This method allowed for the accurate calculation of temperature and heat flux anywhere within the material, at any time.

Chaudhri et al. [9] investigated the thermal transient behavior of a racetrack coil of a quasi-poloidal stellarator when pulsed with high-ampere currents to generate magnetic field. A computer model was developed using finite elements scheme to determine hotspots and heat flux distribution. Assuming natural convective boundary conditions, the rate of cooling was determined and optimal design location of the cooling lines was confirmed. Experiments were also carried out to determine the property data for the copper-glass-epoxy composite conductor coil used in the computational analysis.

In most of the studies reviewed above, the various methods used included the eigenfunction expansion technique, the Green's function approach, the Laplace transform

method, and the Fourier series approach. These methods were used to determine the transient temperature profile when the boundary conditions were specified. However, in the composite coils of the QPS, only the initial conductor temperature and inlet water temperature are known. The actual temperature gradient in the radial direction of the long conductor, approximately 37 m, is also not of much interest. The most relevant pieces of information in the design of the QPS modular coils are the time it takes to cool the conductor to its initial temperature and its dependence on the water flow rate and inlet water temperature. Such information can easily be obtained with reasonable accuracy from a lumped transient analysis as shown by the studies presented below.

Kandala [11] studied the cooling behavior of a racetrack coil of a QPS when heated from room temperature to some specified temperature and internally cooled back to room temperature. A lumped analysis model developed by Narasimhaswami [12] was modified by introducing a heat resistance parameter to account for the effect of temperature gradient across the conductor width. It was shown that the model provided a good engineering tool for understanding the cooling behavior of long conductors when compared with experiments. The analysis was done considering only heat transfer due to radial conduction of the coil. However, considering the large conductivity in the axial direction, 320 W/(mK), compared to that in the radial direction, 9.9 W/(mK), this could be an oversimplification of the problem. This thesis addressed that issue.

3. MATERIALS AND METHODS

3.1 Conductor

The conductor is made of flexible strands of copper wire and a copper tube in the middle. The conductor has a square cross-section of 0.45 in x 0.45 in with the copper tube of 3/16-in inside diameter in the middle as shown in Figure 3.1 below. It is wrapped with fiber glass cloth to serve as electrical insulation and received wound on a spool from the manufacturer.

The following procedure was used to make the 12.2 m conductor for the experiment:

1. Place Ground wrap/Insulation on a cylindrical stainless steel form,
2. Wind conductor,
3. Vacuum impregnation of a polymer, and
4. Heat and Cure.

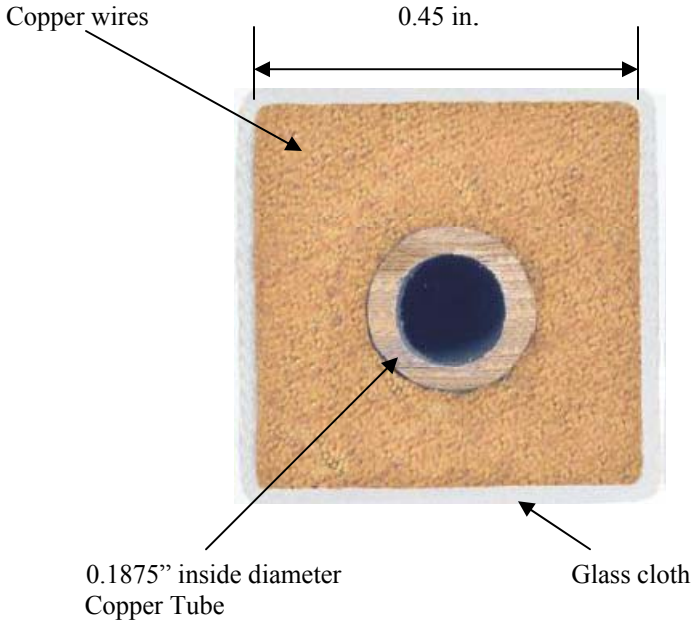

Figure 3.1 Enlarged cross-sectional view of the conductor.

3.1.1 Ground wrap/insulation:

A circular stainless steel winding form of outer and inner radii of approximately 8 and 5 inches, respectively, having a web and flange was used as shown in Figure 3.2. The height of the form was 6 inches. The winding form was cleaned with alcohol to remove all oils, grease and foreign particles. A lakeshore VGE-7031 electrical varnish was brushed evenly on half of the winding form on both the web and flange surfaces to provide the first layer of insulation. After 20 minutes (vanish dry) a second coat was applied and allowed to cure overnight. Kapton adhesive was applied to the other half of the winding form. This approach was taken to demonstrate two different concepts for ground plane. Finally, teflon adhesive tape was applied over the varnished and kapton surfaces to create a slip plane.

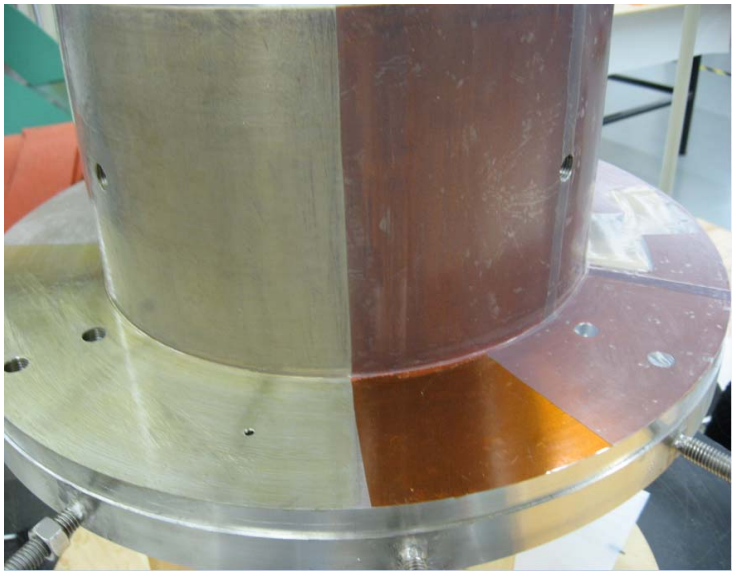

Figure 3.2 Steel winding form with insulation applied.

3.1.2 Winding of conductor:

The conductor was wound in pairs vertically creating a stack of 12. There were six vertical stacks of conductor. Figure 3.3 shows the winding packs of conductor. After winding the stacks of conductor onto the winding form, they were connected and grouped into 12.2 m and 25 m long conductors for the experiment. Thermocouples were placed at the respective locations of the conductor for temperature recordings. They were held in contact with a 3M Scotch-Weld CA40H and then wrapped tightly with kapton tape. A vacuum shield was installed across and around all exposed conductor on the winding form. It consisted of a first layer of Teflon self-adhesive tape, a second layer of glass cloth, a third layer of epoxy hysol brushed on, and a final layer of RTV-736. Upon completion of this procedure, the conductor was ready for vacuum impregnation.

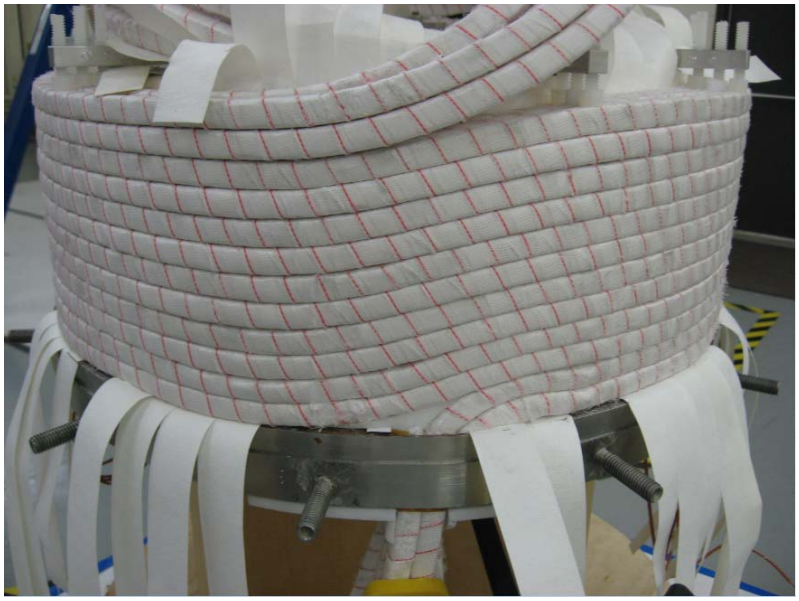

Figure 3.3 Conductor wound on the winding form.

3.1.3 Vacuum Impregnation:

The circular coil winding form was mounted on oven door. One quarter inch NPT brass barbed hose fittings were placed in the delivery/pumping ports. Tygon tubes were connected from the delivery manifold of the 'vacuum impregnation system' to the winding form and from the winding form to the vacuum manifold at hose fittings. Figure 3.4 shows the delivery system. Control valves were opened and closed in a systematic order to allow polymer to flow and wash through and around the conductor. After the impregnation was completed, the coil was allowed to "soak" overnight to assure total saturation.

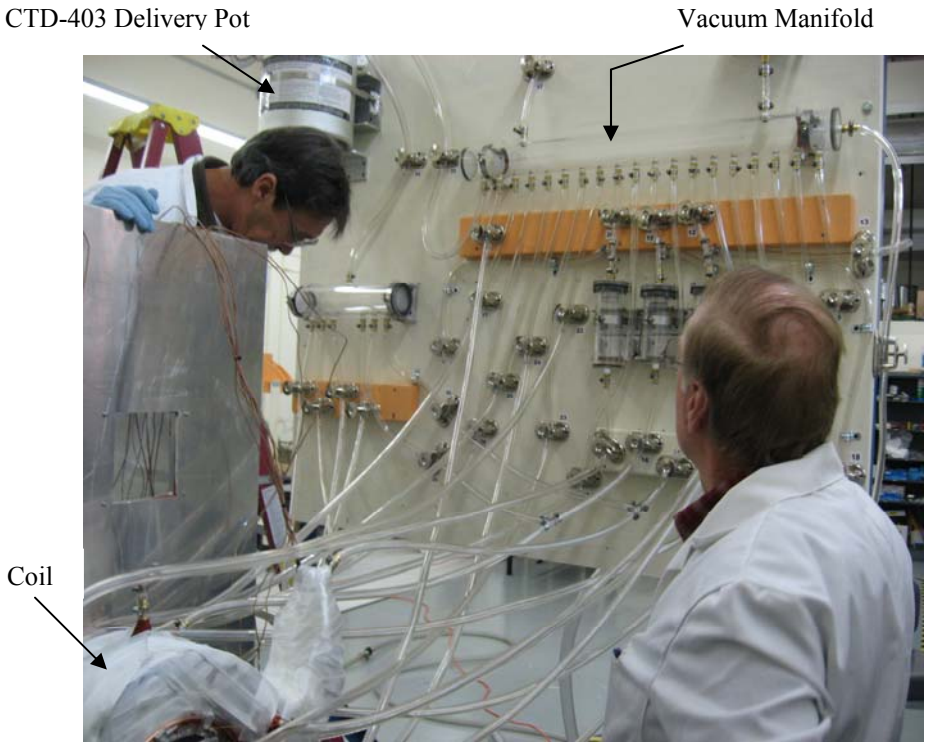

Figure 3.4 Vacuum Impregnation System. Conductor is mounted on oven door and has tygon tube connections to the Vacuum Impregnation System.

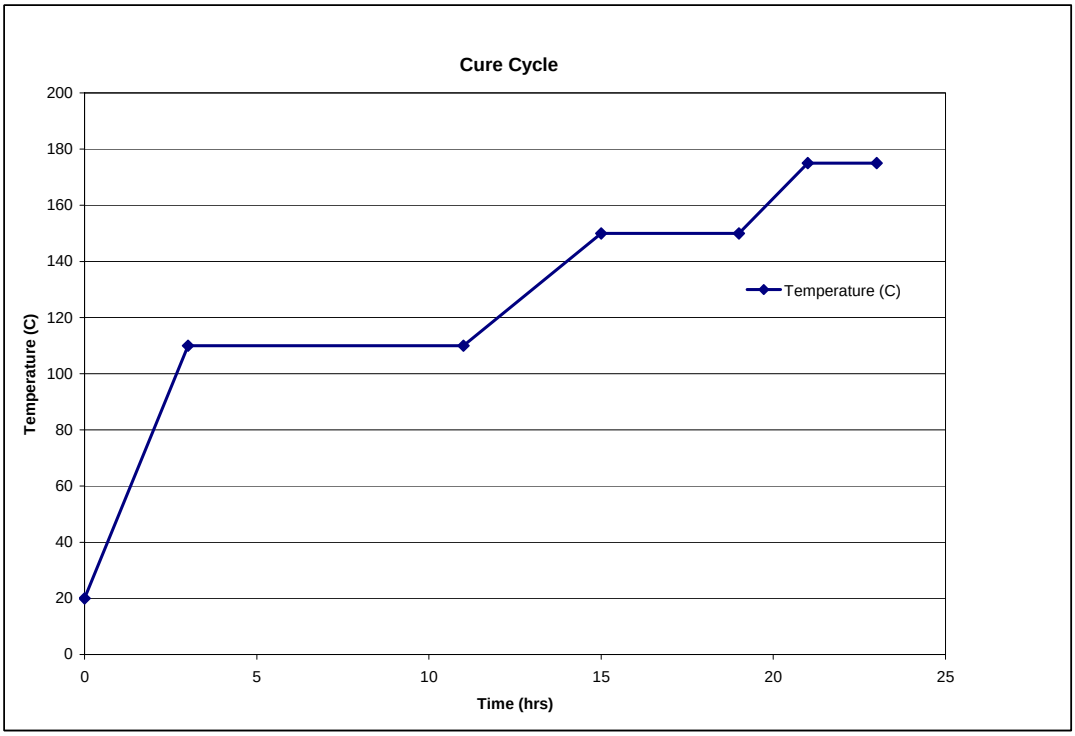

Figure 3.5 Curing cycle used for the polymer.

3.1.4 Heating and Curing:

Curing of the polymer was carried out in accordance with the recommended cure cycle for CTD-403. The cure cycle consisting of several ramp and soak cycles is shown in Figure 3.5 above.

The conductor packs were connected and grouped into 12.2 m and 25 m long lengths for two sets of experiment. Somehow during the experiment, it was realized that the copper tube in the 25 m long conductor (the one on the outermost end of the circular winding form) had been clogged with the polymer during the curing cycle. As such, the experiment had to be modified since the 25 m long conductor was not useable. All the eight thermocouples were removed and new locations were found for them.

Modifications were made by connecting the remaining unclogged stacks of conductor in pairs to form three groups, each of length 12.2 m and each pair was named as

follows: pie 1 (closest to the innermost part of the winding form), pie 2, and pie 3 (on the outermost part). Figure 3.6 shows this arrangement. Each pie had a supply and return for water. Thermocouples were placed on all the three sets of the conductors (pie1, pie 2, and pie 3) and the cooling tubes at inlet, 50% of the length from the inlet, and at return. Those were the only easily accessible locations due to the final configuration of the winding. In order to achieve the adiabatic boundary conditions needed around the conductor (i.e. no heat transfer from pie 2 to its surrounding material), water was sent through pies 1 and 3 at the same rate as pie 2 during the experiments.

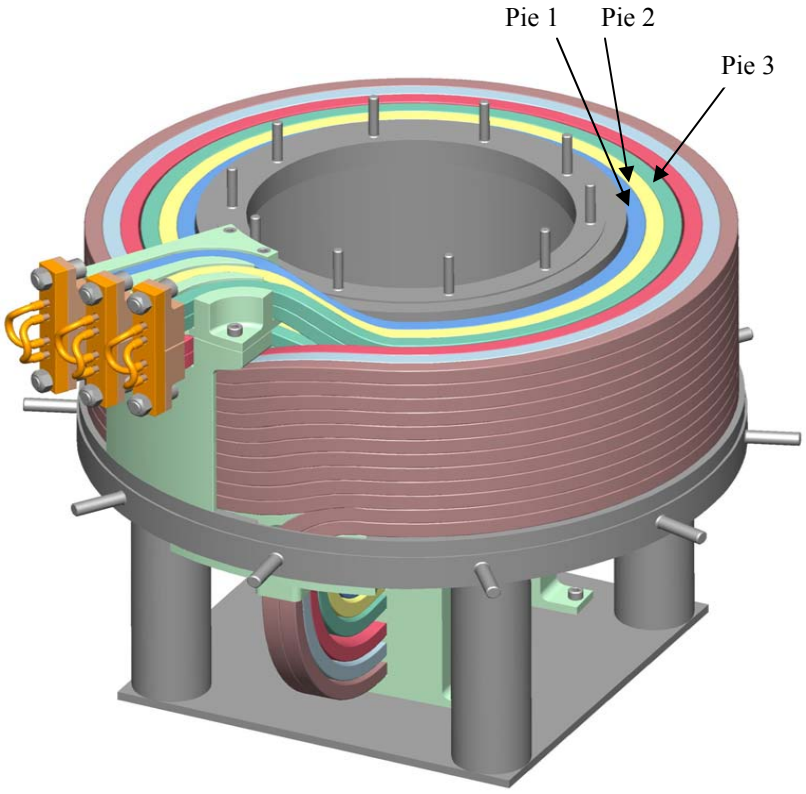

Figure 3.6 Pie arrangement of 12.2 m conductor sets for experiment. Pie 1 is closest to the inside wall (blue color); Pie 2 is in the middle (yellow color); and Pie 3 is the next (green color). The remaining sets are the ones that got clogged.

3.2 Experimental Setup

The experimental setup shown in Figure 3.7 included an oven, a pump, three flow meters (one for each pie), pressure gauges, valves, switches, hoses, data logger, two laptops (one for the oven temperature control and the other for recording data from the thermocouples. The temperature from the thermocouples was recorded once every 10 seconds during the heating and once every second during the cooling paths.), and an oven controller. A separate pump had to be used because it was determined that the pressure from the tap water was not high enough to push the water through the cooling tube at the desired flow rates. The Darcy-Weisbach equation [24] was used to calculate the required pressure for selecting the pump and is as follows:

$$\frac{\Delta p}{\rho} = f\frac{L}{D}\frac{V^2}{2g} \tag{3.1}$$

where L is the length of the conductor, D is the diameter of the tube, V is the velocity of flow, g is the acceleration due to gravity, ρ is the density of water for this case, and f is the pipe friction factor, which can be found from [25]

$$f = \frac{0.316}{\mathrm{Re}^{0.25}}, \quad 10{,}000<\mathrm{Re}<100{,}000 \tag{3.2}$$

The working pressures calculated were between 105.473kPa and 133.48kPa. The pump was also fitted with a bypass flow valve to control the water pressure in the pump. Figure 3.8 shows an enlarged view of the individual components used in the experimental setup.

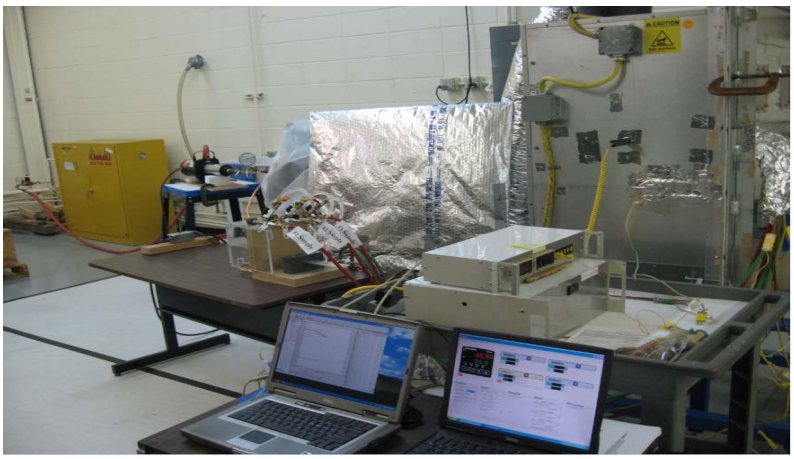

Figure 3.7 Experimental setup used for the experiment.

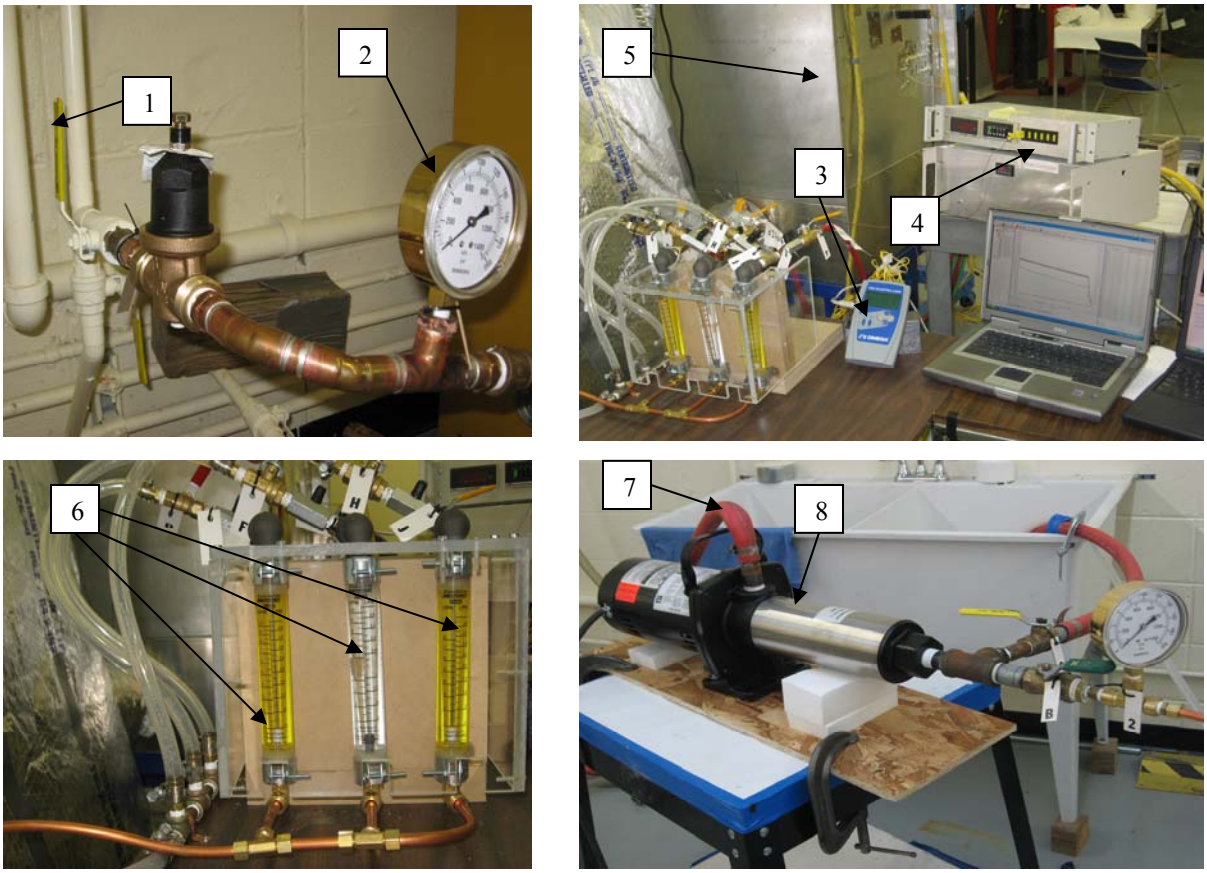

Figure 3.8 Enlarged view of the experimental setup showing individual components. 1) Main water valve; 2) Pressure gauge; 3) Data logger; 4) Oven controller; 5) Forced air convention oven; 6) Flow meters; 7) Hose; 8) Pump.

3.3 Experimental Procedure:

The experiments were conducted to investigate the cooling behavior of the 12.2 m long conductor for flow rates of 0.1, 0.15, 0.2, 0.25, and 0.3 GPM when cooled from temperatures of 60°C and 80°C, which is about the temperatures a QPS coil would be exposed to in operation. The conductor was mounted on the oven door, covered with an insulation blanket and pushed inside the oven. C-clamps were used to secure the oven door. Glass fiber insulation material was placed around all exposed tubes inside and outside of the oven. Figure 3.9 shows photographs of the steps described above. For safety purposes, a detailed procedure was written and a Job Hazards Analysis (JHA)

prepared to discuss any hazards associated with the experiment. The following procedure was followed during the experiment.



(A) (B)

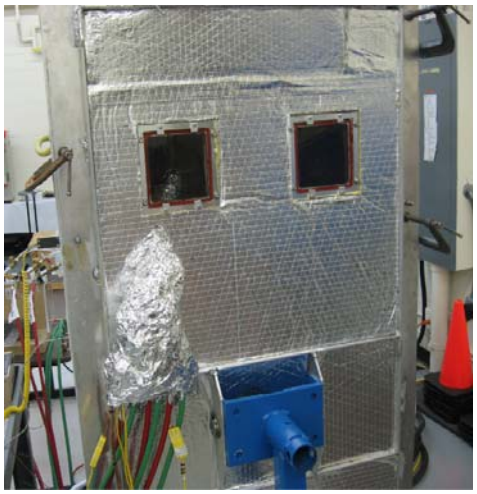

(C)

Figure 3.9 Conductor mounted on oven door (A), Conductor on oven door covered with insulation blanket (B), and Conductor pushed inside oven and door secured with C-clamps. All exposed tubes are covered with insulation material (C).

3.3.1 Heating Process:

The following steps were taken before the heating process began.

1. Open the main water valve to allow water to flow through the pump.
2. Turn the pump on. Adjust the bypass flow valve to ensure that the pressure gauge does not exceed 150 psi.
3. Open all three bypass switches to allow flow into the sink, making sure that all three conductor switches are closed.
4. Adjust all three bypass valves to the desired flow rate.
5. Close all three bypass switches to stop flow into the sink.
6. Open all three conductor switches to allow flow into the conductor.
7. Adjust all three conductor valves to the same flow rate as in step 4.
8. Close all three conductor switches to stop flow into the conductor.
9. Repeat steps 3 and 4 to make sure that the flow rate through the bypass and the conductor remain the same.
10. Turn the pump off.
11. Turn the main valve off to stop flow into the pump.

Once these steps are completed, turn data acquisition on. Set oven temperature to about ten degrees higher than the desired value. Start heating the conductor and set the data acquisition system to record temperatures at the respective thermocouple locations. It took about 20 hours for the conductor temperature to reach the set temperature of 60°C or 80°C.

3.3.2 Cooling Process:

Once the thermocouples reached a temperature about 10 degrees higher than the desired (60°C or 80°C), oven was turned off and water was allowed to flow back in the sink at a set rate without letting it go through the cooling tube. This was done to stabilize the inlet water temperature and to ensure that when the actual cooling started, the inlet water temperature did not change. Once the supply water temperature stabilized, the following steps were taken before letting the water flow through the cooling tubes.

1. Turn the oven off.

2. Allow about 30 minutes for the heating elements to cool and also the conductor temperature to cool down to the desired value (60°C or 80°C). This was necessary to ensure that conductor cooling curves were not affected by the heating elements and the air surrounding the conductor.
3. Close all three bypass switches to prevent flow into the sink.
4. Simultaneously open all the three conductor switches to allow flow into the conductor.
5. Allow conductor to cool down to the supply water temperature.
6. Turn pump off.
7. Turn the main water valve off to stop flow into the pump.

Temperature was recorded at 10-second time intervals for all eight thermocouples during heating and 1-second intervals during cooling of the conductor. A typical result obtained for a flow rate of 0.1 GPM when the conductor cooled from a temperature of 60.2°C is shown in Figure 3.10. From this graph, it can be seen that the temperatures in pie 2 and pie 3 never reached that of pie 1 even after 20 hours of heating. This was due to the winding form acting as a heat sink that was always conducting heat to Pie 1 since it was the closest in contact with it. The "wait period" in Figure 3.10 was used to allow the temperatures to stabilize. The remaining results are shown in Appendix A.

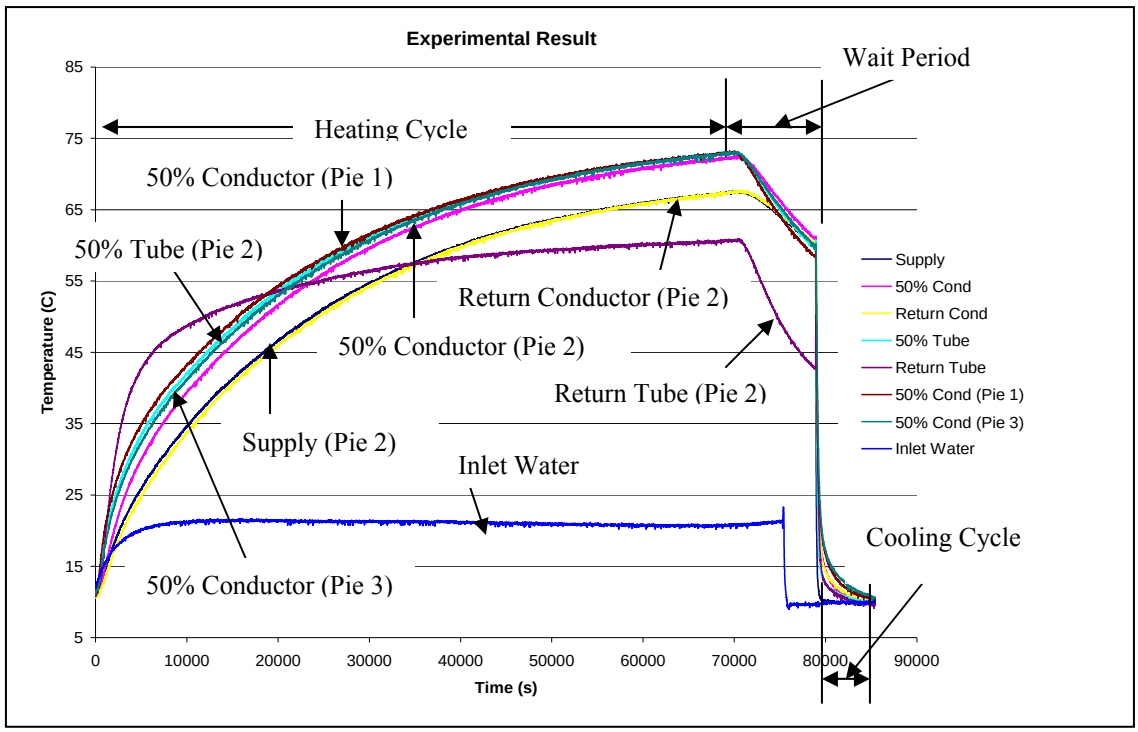

Figure 3.10 A typical experimental results obtained when the conductor was heated to 60.2°C and cooled with water flowing at a rate of 0.1 GPM. The 'heating cycle' refers to the complete heating period, the 'wait period' being the time when the oven elements were allowed to cool down and temperatures allowed to stabilize, and the 'cooling cycle' refers to the duration of cooling by introducing water into the conductor.

4. NUMERICAL SIMULATION

4.1 Elemental Model

In the earlier model developed by Narasimhaswami [12] and modified by Kandala [11], the focus was only on heat transfer due to radial conduction of the coil based on a radially lumped analysis. The effect of axial heat conduction along the length of the conductor was ignored. However, considering the large conductivity in the axial direction, 320 W/(mK), compared to that in the radial direction, 9.9 W/(mK), this could be an oversimplification of the problem. Heat would be conducted both in the radial direction to water elements and in the axial direction to neighboring elements throughout the entire length of the conductor.

In this model, both the composite and water are divided into equal number of elements of uniform length as before. However, the heat transfer process occurs in two directions- radial and axial directions. As such, the analysis is done in two steps- a radial heat transfer analysis followed by an axial heat transfer analysis. Figure 4.1 shows the elements and the respective directions for heat transfer.

In the radial direction, a water element entering the tube will absorb heat from every composite element along its path from the entry until it exits the tube. As it moves through the tube, it is assumed that the water element stops for an incrementally small time, called time step, to remove heat from the composite elements. The time step depends on the flow rate. In a particular time step, the radial heat transfer analysis allows for calculation of the final temperatures of all composite elements after interacting with the water elements.

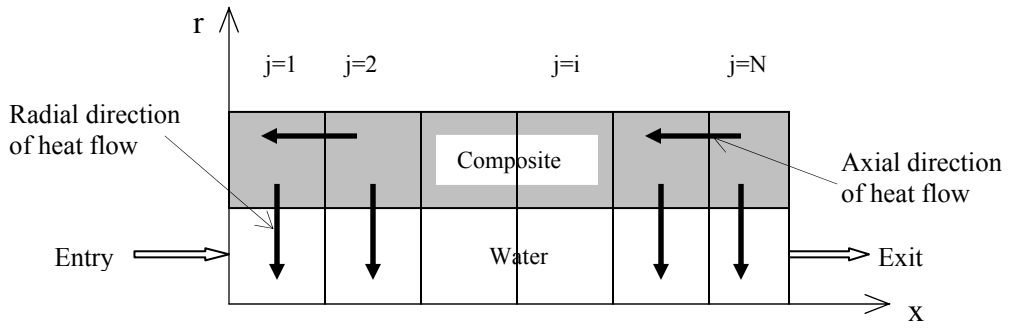

Figure 4.1 Elemental model. The direction of heat flow is shown by solid arrows.

4.2 Radial conduction analysis

Let us consider a water element entering the left end of the tube at a temperature T_{iwater}. When it comes in contact with the first element for an incremental time step, it will remove heat from the 1st composite element. It then moves to the next composite element. The temperature of this water element will increase during the time step. This new elevated temperature becomes the initial temperature of water element in contact with the 2nd composite element at the next time step. The process of heat removal continues as fresh water keeps entering the tube until the composite is eventually cooled after some given length of time.

The final temperature of a composite element after interacting with a water element can be obtained from the following equation [11]:

$$\frac{T_{fcomp} - T_{iwater}}{T_{icomp} - T_{iwater}} = e^{-Bi \times Fo} \tag{4.1}$$

where

T_{fcomp} is the final temperature of composite element after interacting with water element,

T_{icomp} is the initial temperature of composite,

T_{iwater} is the initial temperature of water,

Bi is the Biot number ($Bi = hL_c/k_r$ where h is the average convective heat transfer coefficient, L_c is the length of conductor, k_r is the thermal conductivity of the composite

in the radial direction, which is 9.9 W/(mK)and Fo is the Fourier number (Fo = $\alpha t/L_c$ where α = thermal diffusivity, t = time step).
Once the final temperature of the composite element is known, the final temperature of the water element can be obtained using the conservation of energy as:

Heat lost from composite element = Heat gained by the water element

$$-m_{comp} \times C_{pcomp} \times \left(T_{icomp} - T_{fwater}\right) = m_{water} \times C_{pwater} \times \left(T_{iwater} - T_{fwater}\right) \quad (4.2)$$

where

T_{fwater} is the final temperature of water,

m_{comp} is the mass of a composite element,

m_{water} is the mass of a water element,

C_{pcomp} is the specific heat capacity of the composite,

C_{pwater} is the specific heat capacity of water.

This water element with an elevated temperature moves to the next position and interacts with the next composite element based on the same assumptions above.

During a particular time step, once the radial heat transfer analysis is completed, the final temperature of all composite elements will be known. This part of the analysis described so far is for the heat transfer in the radial direction only and was developed by Narasimhaswami [12] and modified by Kandala [11]. However, these elements are in perfect thermal contact and transfer heat from one to another throughout the entire length of the conductor. To account for this heat transfer occurring between the composite elements, an axial heat transfer analysis is required. The following sections describe this contribution to the model.

4.3 Axial conduction analysis

In the axial heat transfer analysis, three adjacent composite elements are considered at a time. They are assumed to be thermally insulated from the rest of the elements, as shown in Figure 4.2, and allowed to interact during the time step so that their temperatures are updated according to the variation of parameters procedure outlined below [25].

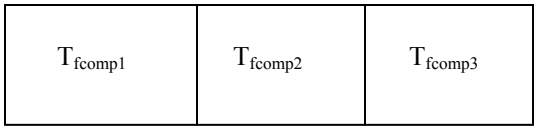

Figure 4.2 Three composite elements.

The problem is modeled as a transient conduction heat transfer with the following formulation, with representation shown in Figure 4.3 (a).

Governing equation: $\frac{\partial^2 T}{\partial x^2} = \frac{1}{\alpha}\frac{\partial T}{\partial t}$ in $0 \le x \le L$ for $t \ge 0$ (4.3a)

Boundary conditions: $T(0,t) = T_{fcomp1}$ for $t > 0$ (4.3b)

$T(L,t) = T_{fcomp3}$ for $t > 0$

Initial condition: $T(x,0) = T_{fcomp2}$, $x \in [0,L]$ (4.3c)

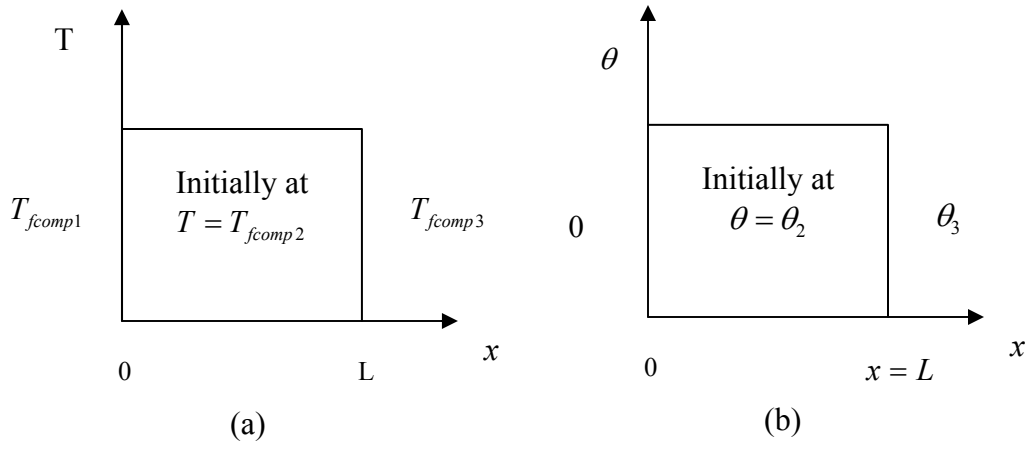

Figure 4.3 Representation of the problems. (a) description of the problem using equations 4.3, (b) description of the problem using equations 4.8

Solution procedure [24]:

Making a temperature shift,

Let $\theta = T - T_{fcomp1}$ (4.4)

$$\Rightarrow T(x,t) = \theta + T_{fcomp1} \tag{4.5}$$

$$\Rightarrow \frac{\partial T}{\partial t} = \frac{\partial \theta}{\partial t} \text{ and } \frac{\partial T}{\partial x} = \frac{\partial \theta}{\partial x}, \tag{4.6}$$

$$\Rightarrow \frac{\partial^2 T}{\partial x^2} = \frac{\partial^2 \theta}{\partial x^2} \tag{4.7}$$

Consequently,

$\theta_1 = T_{fcomp1} - T_{fcomp1} = 0$, $\theta_2 = T_{fcomp2} - T_{fcomp1}$, and $\theta_3 = T_{fcomp3} - T_{fcomp1}$

Substituting these expressions into the original problem results in a problem formulation as follows, (representation is shown in Figure 4.3 (b)):

Governing equation: $\frac{\partial^2 \theta}{\partial x^2} = \frac{1}{\alpha}\frac{\partial \theta}{\partial t}$ in $0 \le x \le L$ for $t \ge 0$ (4.8a)

Boundary conditions: $\theta(0,t) = 0$ for $t > 0$ (4.8b)

$\theta(L,t) = \theta_3$ for $t > 0$

Initial condition: $\theta(x,0) = \theta_2,\ x \in [0,L]$ (4.8c)

Now to get the eigenvalues and eigenfunction, we simply set all the nonhomogeneous terms in equations 4.8 equal to zero (i.e $\theta_3 = 0$), to yield a corresponding homogeneous problem. Then the variables can be separated in the corresponding homogeneous problem as follows:

Assume

$$\theta(x,t) = X(x)T(t) \tag{4.9}$$

Taking the respective derivatives and substituting into equation (4.8a) we obtain

$$X''T = \frac{1}{\alpha} XT' \tag{4.10}$$

$$\Rightarrow \frac{X''}{X} = \frac{T'}{\alpha T} = -\lambda^2 \tag{4.11}$$

The eigenfunctions X are thus obtained from

$$X'' + \lambda^2 X = 0 \tag{4.12}$$

subject to the boundary conditions

$$X(0) = 0 \quad \text{and} \quad X(L) = 0 \tag{4.13}$$

The solution for X is

$$X = A\cos\lambda x + B\sin\lambda x \tag{4.14}$$

The boundary condition at $x = 0$ yields

$$A = 0$$

The boundary condition at $x = L$ yields

$$0 = B\sin\lambda L \quad \text{or} \quad \sin\lambda L = 0$$

$$\Rightarrow \lambda_n = \frac{n\pi}{L}, \qquad n = 1,2,3,... \tag{4.15}$$

Therefore, the eigenfunctions of the corresponding homogeneous problem are

$$X_n(x) = \sin\frac{n\pi x}{L}, \qquad n = 1,2,3,... \tag{4.16}$$

From superposition principle, a solution can be constructed in the form

$$\theta(x,t) = \sum_{n=1}^{\infty} A_n(t)\sin\frac{n\pi x}{L}, \qquad x \in [0, L],\ t \geq 0 \tag{4.17}$$

where $A_n(t)$ is a constant to be determined as a function of *t*.

Applying inner product

$$\int_0^L \theta(x,t)\sin\frac{m\pi x}{L}dx = \sum_{n=1}^{\infty} A_n(t)\int_0^L \sin\frac{n\pi x}{L}\sin\frac{m\pi x}{L}dx \tag{4.18}$$

By orthogonality

$$\int_0^L \theta(x,t)\sin\frac{m\pi x}{L}dx = \frac{L}{2}A_m(t) \tag{4.19}$$

$$\Rightarrow\ A_m(t) = \frac{2}{L}\int_0^L \theta(x,t)\sin\frac{m\pi x}{L}dx, \qquad m = 1,2,... \tag{4.20}$$

Differentiating with respect to time gives

$$\frac{dA_m(t)}{dt} = \frac{2}{L}\int_0^L \frac{\partial\theta(x,t)}{\partial t}\sin\frac{m\pi x}{L}dx, \tag{4.21}$$

$$\text{but}\ \frac{\partial\theta}{\partial t} = \alpha\frac{\partial^2\theta}{\partial x^2} \tag{4.22}$$

$$\therefore\quad \frac{dA_m(t)}{dt} = \frac{2\alpha}{L}\int_0^L \frac{\partial^2\theta}{\partial x^2}\sin\frac{m\pi x}{L}dx, \qquad m = 1,2,... \tag{4.23}$$

Integrating by parts twice gives

$$\frac{dA_m(t)}{dt} = \frac{2\alpha}{L}\left\{\left[\frac{\partial\theta}{\partial x}\sin\frac{m\pi x}{L}\right]_0^L - \frac{m\pi}{L}\int_0^L \frac{\partial\theta}{\partial x}\cos\frac{m\pi x}{L}dx\right\}$$

$$= \frac{-2\alpha m\pi}{L^2}\int_0^L \frac{\partial\theta}{\partial x}\cos\frac{m\pi x}{L}dx$$

$$= \frac{-2\alpha m\pi}{L^2}\left\{\left[\theta(x,t)\cos\frac{m\pi x}{L}\right]_o^L + \frac{m\pi}{L}\int_0^L \theta(x,t)\sin\frac{m\pi x}{L}dx\right\}$$

$$= \frac{-2\alpha m\pi}{L^2}\left[\theta(L,t)\cos m\pi - \theta(0,t)\right] - \frac{2\alpha m^2\pi^2}{L^3}\int_0^L \theta(x,t)\sin\frac{m\pi x}{L}dx$$

$$= \frac{-2\alpha m\pi}{L^2}\left[\theta(L,t)\cos m\pi - \theta(0,t)\right] - \frac{\alpha m^2\pi^2}{L^2}A_m(t), \quad m = 1,2,... \tag{4.24}$$

Then

$$\frac{dA_m(t)}{dt}+\frac{\alpha m^2\pi^2}{L^2}A_m(t)=\frac{-2\alpha m\pi}{L^2}\left[\theta(L,t)\cos m\pi-\theta(0,t)\right],\quad m=1,2,... \tag{4.25}$$

$$\frac{d}{dt}\left(A_m(t)e^{\frac{\alpha m^2\pi^2 t}{L^2}}\right)=\frac{-2\alpha m\pi}{L^2}e^{\frac{\alpha m^2\pi^2 t}{L}}\left[\theta(L,t)\cos m\pi-\theta(0,t)\right] \tag{4.26}$$

Integrating gives

$$A_m(t)e^{\frac{\alpha m^2\pi^2 t}{L^2}}=\frac{-2}{m\pi}e^{\frac{\alpha m^2\pi^2 t}{L}}\left[\theta(L,t)\cos m\pi-\theta(0,t)\right]+C_m,\ C_m=\text{constant},\ m=1,2,... \tag{4.27}$$

Substituting known terms into equation (4.27) gives

$$A_m(t)e^{\frac{\alpha m^2\pi^2 t}{L^2}}=\frac{-2}{m\pi}e^{\frac{\alpha m^2\pi^2 t}{L}}\left[\theta_3\cos m\pi\right]+C_m \tag{4.28}$$

$$\therefore\quad A_m(t)=\frac{-2}{m\pi}\theta_3\cos m\pi+C_m e^{-\frac{\alpha m^2\pi^2 t}{L^2}},\quad m=1,2,... \tag{4.29}$$

Applying the initial condition: At $t=0$, $\theta(x,0)=\theta_2$ we get

$$A_m(0)=\frac{-2}{m\pi L}\left[\theta_3\cos m\pi\right]+C_m,\qquad m=1,2,... \tag{4.30}$$

Also from equation (4.20)

$$A_m(t)=\frac{2}{L}\int_0^L\theta(x,t)\sin\frac{m\pi x}{L}dx,\qquad m=1,2,... \tag{4.31}$$

$$\therefore\quad A_m(0)=\frac{2}{L}\int_0^L\theta(x,0)\sin\frac{m\pi x}{L}dx=\frac{2\theta_2}{L}\int_0^L\sin\frac{m\pi x}{L}dx=\left[\frac{-2\theta_2}{m\pi}\cos\frac{m\pi x}{L}\right]_0^L \tag{4.32}$$

$$\Rightarrow A_m(0)=\frac{-2\theta_2}{m\pi}\cos m\pi+\frac{2\theta_2}{m\pi}=\frac{2\theta_2}{m\pi}\left[1-\cos m\pi\right],\quad m=1,2,... \tag{4.33}$$

From equations (4.30) and (4.33)

$$C_m=\frac{2\theta_2}{m\pi}\left[1-\cos m\pi\right]+\frac{2\theta_3}{m\pi}\cos m\pi=\frac{2}{m\pi}\left[\theta_2\left(1-\cos m\pi\right)+\theta_3\cos m\pi\right] \tag{4.34}$$

Substituting into equation (4.29) gives

$$A_m(t)=\frac{-2}{m\pi}\theta_3\cos m\pi+\frac{2}{m\pi}\left[\theta_2\left(1-\cos m\pi\right)+\theta_3\cos m\pi\right]e^{-\frac{\alpha m^2\pi^2 t}{L^2}} \tag{4.35}$$

Thus

$$\theta(x,t)=\sum_{n=1}^{\infty}A_n(t)\sin\frac{n\pi x}{L} \tag{4.36}$$

$$=\sum_{n=1}^{\infty}\left\{\frac{-2}{n\pi}\theta_3\cos n\pi+\frac{2}{n\pi}\left[\theta_2\left(1-\cos n\pi\right)+\theta_3\cos n\pi\right]e^{-\frac{\alpha n^2\pi^2 t}{L^2}}\right\}\sin\frac{n\pi x}{L} \tag{4.37}$$

$$=\sum_{n=1}^{\infty}\frac{-2}{n\pi}\theta_3\cos n\pi\sin\frac{n\pi x}{L}+\sum_{n=1}^{\infty}\frac{2}{n\pi}\left[\theta_2\left(1-\cos n\pi\right)+\theta_3\cos n\pi\right]\sin\left(\frac{n\pi x}{L}\right)e^{-\frac{\alpha n^2\pi^2 t}{L^2}} \tag{4.38}$$

But,

$$T(x,t)=\theta(x,t)+T_{fcomp1} \tag{4.39}$$

$$=T_{fcomp1}+\sum_{n=1}^{\infty}\frac{-2}{n\pi}\theta_3\cos n\pi\sin\frac{n\pi x}{L}$$

$$+\sum_{n=1}^{\infty}\frac{2}{n\pi}\left[\theta_2\left(1-\cos n\pi\right)+\theta_3\cos n\pi\right]\sin\left(\frac{n\pi x}{L}\right)e^{-\frac{\alpha n^2\pi^2 t}{L^2}},\ x\in[0,L],\ t\geq 0 \tag{4.40}$$

Note that α is the thermal diffusivity ($\alpha = k_x/(\rho C_p)$ where k_x is the thermal conductivity in the axial direction of the conductor, which is 320W/(mK), ρ is the density, and C_p is the specific heat capacity). Equation (4.40) gives the updated temperature profile of the middle element of the three element composite slab under time invariant boundary conditions. However, this series solution is not uniformly convergent at x = 0, L.

But,

$$\sum_{n=1}^{\infty}\frac{\cos n\pi}{n}\sin\frac{n\pi x}{L}=\sum_{n=1}^{\infty}\frac{(-1)^n}{n}\sin\left(\frac{n\pi x}{L}\right)=-\frac{\pi x}{2L},\qquad x\in[0,L] \tag{4.41}$$

Making the appropriate substitutions, equation (4.40) reduces to

$$T(x,t)=T_{fcomp1}-\frac{2\theta_3}{\pi}\left(-\frac{\pi x}{2L}\right)$$

$$+\frac{2\theta_2}{\pi}\sum_{n=1}^{\infty}\left[\left(1-(-1)^n\right)+\frac{\theta_3}{\theta_2}(-1)^n\right]\sin\left(\frac{n\pi x}{L}\right)e^{-\frac{\alpha n^2\pi^2 t}{L^2}},\quad x\in[0,L],\ t\geq 0 \tag{4.42}$$

which is uniformly convergent and a physically better solution that matches Figure 4.4 at t = 0, x = 0, x = L, and $t\to\infty$. Hence, equation (4.42) gives the updated temperature profile of the middle element of the three element composite slab under time invariant

boundary conditions. The area, A_{comp2}, under this graph in Figure 4.4 (b), can be found from trapezoid rule or simply by direct integration.

$$A_{comp2} = \int_0^L T(x,t)dx \equiv T_{upcomp2} * L \tag{4.43}$$

$$\Rightarrow T_{upcomp2} = \frac{A_{comp2}}{L} \tag{4.44}$$

This gives the updated average temperature of the middle element in the three elements composite after the interaction. During interaction with elements on both sides, the middle element assumes typical temperature profiles in Figure 4.4 for the various times: initial time, small times, and large times.

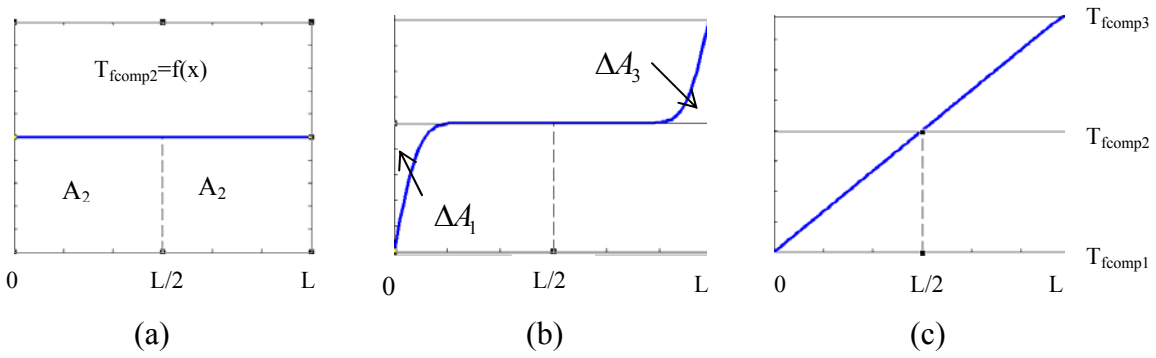

Figure 4.4 Typical temperature profile of the middle element for various times during the interaction with neighboring elements: (a) time = 0; (b) time = 0.01 sec.; (c) time = 1 sec.

For the time t = 0, Figure 4.4 (a) shows that the area under this temperature profile is

$$A = 2A_2 = T_{fcomp2} \times L \tag{4.45}$$

thus the area, $A_2 = \frac{1}{2}\left(T_{fcomp2} \times L\right)$ (4.46)

For small times, the graph shows an increasing slope to the right side and a decreasing slope to the left, Figure 4.4 (b). The area ΔA_1 is proportional to the heat lost by composite element number 2 to number 1, and area ΔA_3 is proportional to the heat gained by composite element number 2 from number 3. Area under this temperature profile is

$$A_{comp2} = \int_0^L T(x,t)dx = \int_0^{L/2} T(x,t)dx + \int_{L/2}^L T(x,t)dx \equiv T_{fcomp2} * L \tag{4.47}$$

From an energy analysis,

area, $\Delta A_1 \equiv$ Heat lost from the middle element to the left element

area, $\Delta A_3 \equiv$ Heat transferred from the right element to the middle element

Now let

$$A_1 = \int_0^{L/2} T(x,t)dx \tag{4.48}$$

$$A_3 = \int_{L/2}^L T(x,t)dx \tag{4.49}$$

$$\Rightarrow A_{comp2} = A_1 + A_3 \tag{4.50}$$

Then

$$\Delta A_1 = A_2 - A_1 \tag{4.51}$$

and

$$\Delta A_3 = A_3 - A_2 \tag{4.52}$$

From the geometry, the updated temperature of the left element is found from

$$T_{upcomp1} * L = T_{fcomp1} * L + \Delta A_1 \tag{4.53}$$

$$\Rightarrow T_{upcomp1} = \frac{T_{fcomp1} * L + \Delta A_1}{L} \tag{4.54}$$

and the updated temperature of the right element is also found from

$$T_{upcomp3} * L = T_{fcomp3} * L - \Delta A_3 \tag{4.55}$$

$$\Rightarrow T_{upcomp3} = \frac{T_{fcomp3} * L - \Delta A_3}{L} \tag{4.56}$$

Once each of these three composite elements has their temperatures updated, the next three adjacent elements are considered and treated the same way to update their temperatures. This process continues for the entire length of the conductor giving the updated temperatures after the axial heat transfer.

In the next time step, the cooling process continues as fresh water elements are introduced into the tube to interact with previously cooled composite elements in the radial direction and then the axial direction heat transfer follows. This continues until the entire length of the conductor cools down to the initial water temperature.
This numerical lumped model was developed in MATLAB-7. The number of elements used in the computations was 1000. Using more than 1000 elements did not vary the results significantly. The difference between using 1000 and 10,000 elements was less than 1%. However, a significant difference varying from 5% to 10% was seen between the results of 1000 elements and less than that (900, 800, and 500) [9]. As such, 1000 elements were used in all the numerical simulations to cool the entire conductor down to within 1°C of the inlet water temperature. The thermal properties of the Cu/Cyanate Ester composite conductor were determined experimentally at the High Temperature Materials Testing Laboratory of Oak Ridge National Laboratory [26]. Table 4.1 shows the properties of the conductor.

Table 4.1 Properties of the conductor used in the lumped model.

Property		Composite Conductor	Water
Density (kg/m^3)		7400	1000
Thermal Conductivity (W/(mK))	in the radial direction	9.9	0.625
	in the axial direction	320	
Specific Heat (J/(kg.K))		404	4200

5. RESULTS AND DISCUSSIONS

5.1 Overview

The discussion in this section is divided into two parts. The first part discusses the effect of inclusion of axial conduction on the model predictions. The second part of the section compares the lumped model predictions (accounting for the effect of axial conduction between conductor elements) with the experimental results.

5.1.1 Investigating the effect of axial conduction on the lumped model

In order to investigate the significance of axial conduction in the lumped model, the numerical and experimental results generated by Kandala [11] for the 5.5 m long conductor, were compared with those generated from the lumped model accounting for axial conduction between conductor elements (we shall call it LMAC) in this thesis. A radial heat resistance parameter (as defined in Kandala [11]) of 9 mm was used and the results are shown in Figures 5.1-5.2.

Conductor Length = 5.5 m, Water Flow Rate = 0.1 GPM, Conductor Initial Temperature = 61.6°C, Water Inlet Temperature = 18°C, Heat Resistance Parameter = 9 mm

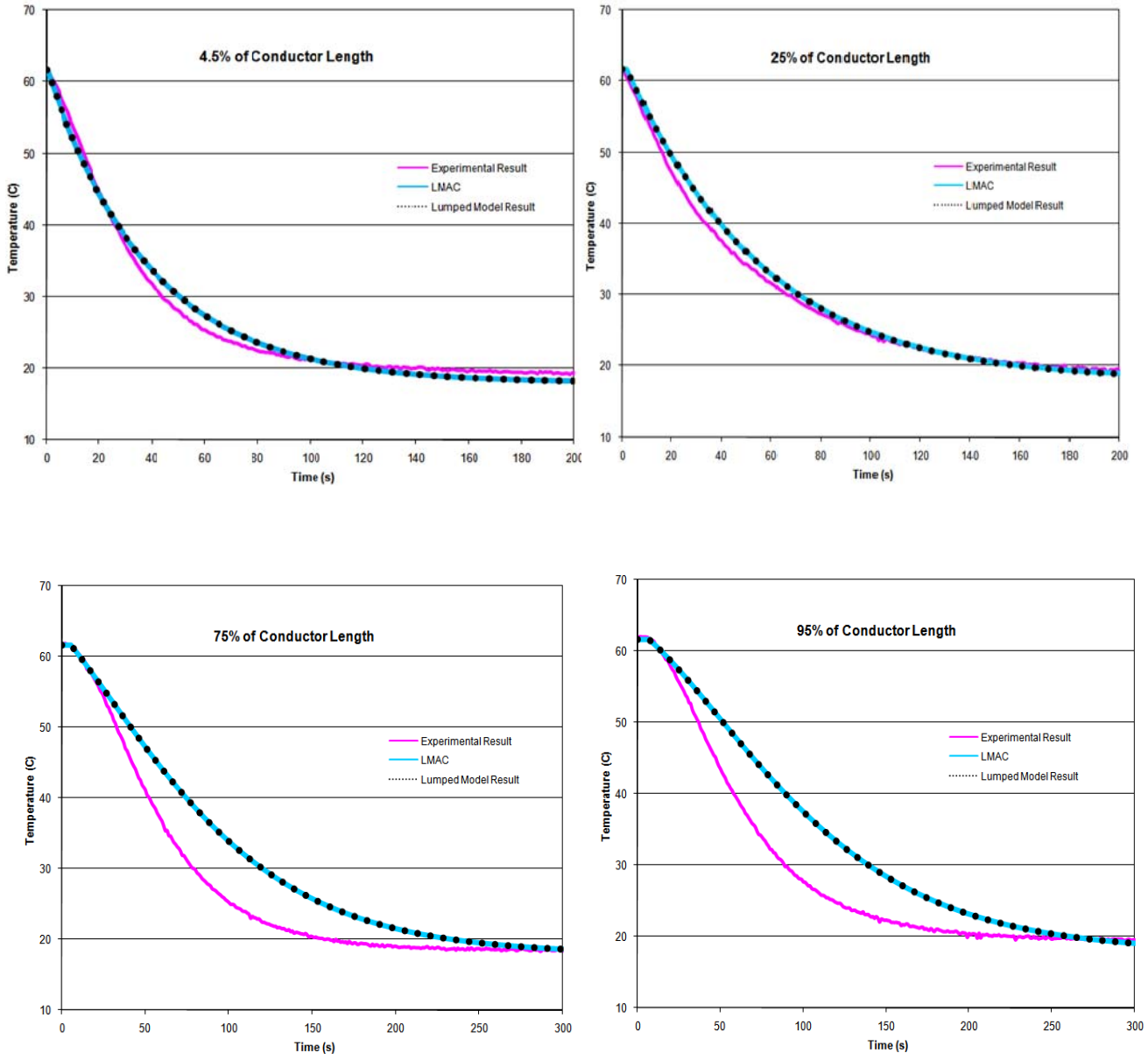

Figure 5.1 Comparisons between experimental and predicted cooling curves (at locations of 4.5%, 25%, 75%, and 95% of the conductor length) for lumped model and lumped model with axial conduction when a 5.5m long conductor was cooled by 18°C water flowing through the cooling tube at 0.1GPM. In all predictions, the heat resistance parameter, L*, was 9 mm.

Conductor Length = 12.2 m, Water Flow Rate = 0.1 GPM, Conductor Initial Temperature = 60.2°C, Water Inlet Temperature = 9.9°C, Heat Resistance Parameter = 9 mm

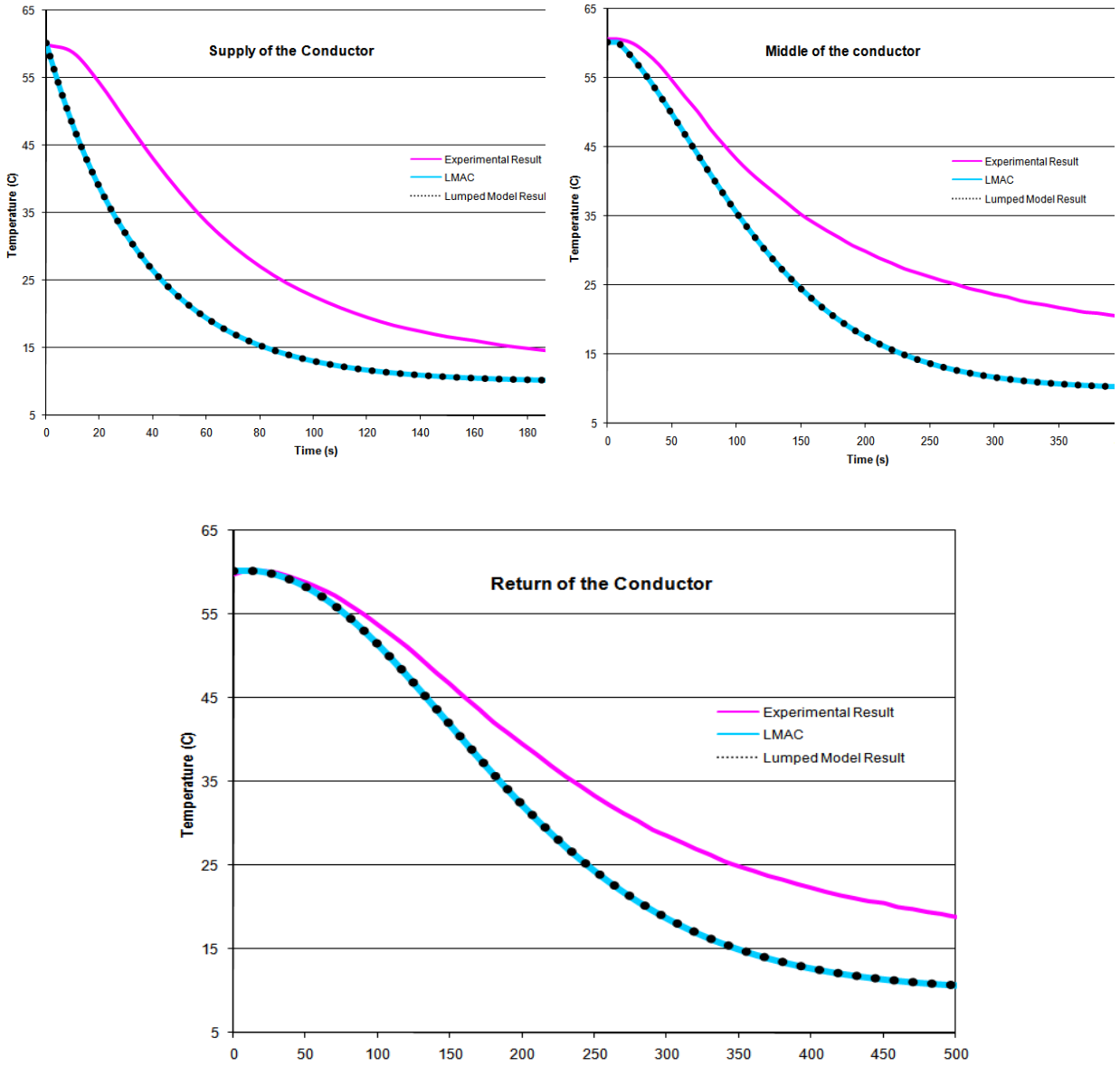

Figure 5.2 Comparisons between experimental and predicted cooling curves (at the supply, middle, and return of the conductor length) for lumped model and lumped model with axial conduction when 12.2m long conductor was cooled by 9.9°C water flowing through the cooling tube at 0.1GPM. In all predictions, the heat resistance parameter, L*, was 9mm.

It can be seen from Figures 5.1 - 5.2 that the two predicted curves- lumped model by Kandala [11] and the modified lumped model in this thesis, LMAC, overlapped each other. This means that the effect of axial conduction was not significant in the heat transfer process for flow rate of 0.1 GPM. In the cases of different lengths of the conductor (5.5 m and 12.2 m), the same trend was seen in the graphs. When a similar analysis was done for flow rates greater than 0.1 GPM, the same effect was seen. However, for flow rates far less than 0.1 GPM, the effect of axial conduction is more visible. A typical result is shown in Figure 5.3 for a flow rate of 0.005 GPM. In these graphs, the LMAC cools slightly faster than the lumped model by Kandala [11]. A magnified result of this trend is shown in Figure 5.4 where the effect is blown up for clear visualization. At very low flow rates, the rate of heat removal from the conductor by the flowing water is much smaller. Hence, the effect of axial conduction is more evident when the flow rate is small. However, at larger flow rates of the cooling water, most of the heat removal from the conductor is in the radial direction by means of the water. While the axial conduction still occurs, its effect in comparison to the radial heat transfer is minimal. Generally, the QPS coils would not be cooled by flow rates far less than 0.1 GPM, making the effect of axial conduction insignificant and could be neglected in the lumped model.

Conductor Length = 5.5 m, Water Flow Rate = 0.005 GPM, Conductor Initial Temperature = 61.6°C, Water Inlet Temperature = 18°C, Heat Resistance Parameter = 9 mm

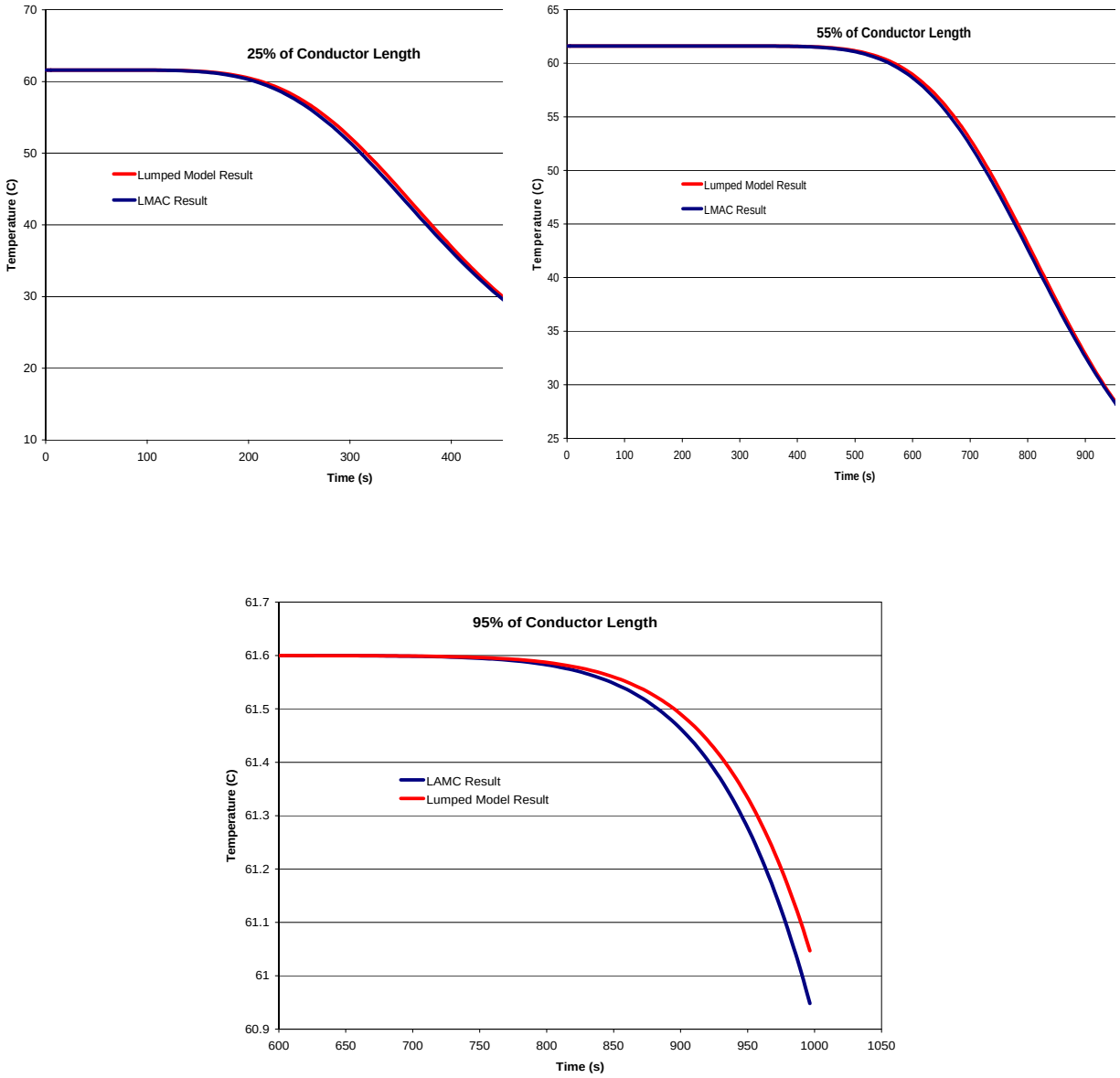

Figure 5.3 Comparisons between predicted cooling curves (at locations of 25%, 55%, and 95% of the conductor length) for lumped model and lumped model with axial conduction when a 5.5m long conductor was cooled by 18°C water flowing through the cooling tube at 0.1GPM. In all predictions, the heat resistance parameter, L*, was 9 mm.

Conductor Length = 5.5 m, Water Flow Rate = 0.005 GPM, Conductor Initial Temperature = 61.6°C, Water Inlet Temperature = 18°C, L* = 9 mm

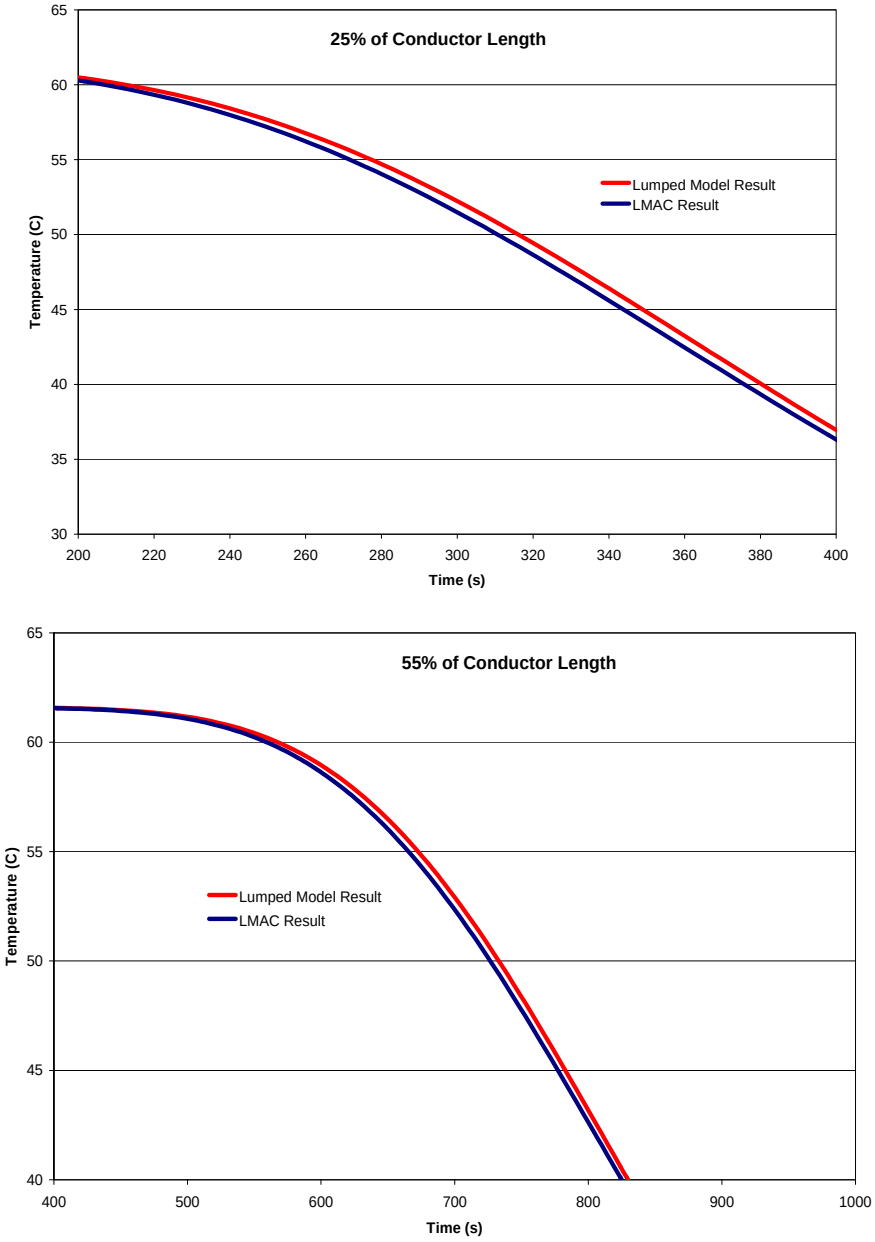

Figure 5.4 Magnified view of Figure 5.3 to clearly show the comparisons between predicted cooling curves (at locations of 25%, and 55% of the conductor length) for lumped model and lumped model with axial conduction when a 5.5m long conductor was cooled by 18°C water flowing through the cooling tube at 0.1GPM. In all predictions, L* was 9 mm.

5.1.2 Comparison between Experimental and LMAC Results

During the experiments, temperature was recorded by four thermocouples placed at different locations of the 12.2 m long conductor (pie 2). These are: at the conductor inlet, at halfway along the conductor, at halfway along the cooling tube, and at the end of the conductor. Since the thermocouple at the end of the conductor was not able to reach the 60°C or 80°C temperature of the conductor before cooling began (see Figure 3.10), its recorded data was discarded for unreliability. The experimental results of the remaining three locations were compared with the predicted results from the LMAC, for five different flow rates of 0.1, 0.15, 0.2, 0.25, and 0.3 GPM. Since there was no difference between the predictions from LMAC and the lumped model for flow rates larger than 0.1 GPM, we shall refer to the LMAC results simply as lumped model results. A total of 30 predicted curves were compared with experimental data.

The section below discusses the results of cooling the conductor from 60°C, and then does the same for 80°C. Figures 5.5-5.9 show representative results from these comparisons when the conductor was cooled from 60°C. Figures 5.10-5.14 show representative results from the comparisons when the conductor was cooled from 80°C.

Conductor Length = 12.2 m, Water Flow Rate = 0.1 GPM, Conductor Initial Temperature = 60.2°C, Water Inlet Temperature = 9.9°C, Heat Resistance Parameter = 9 mm

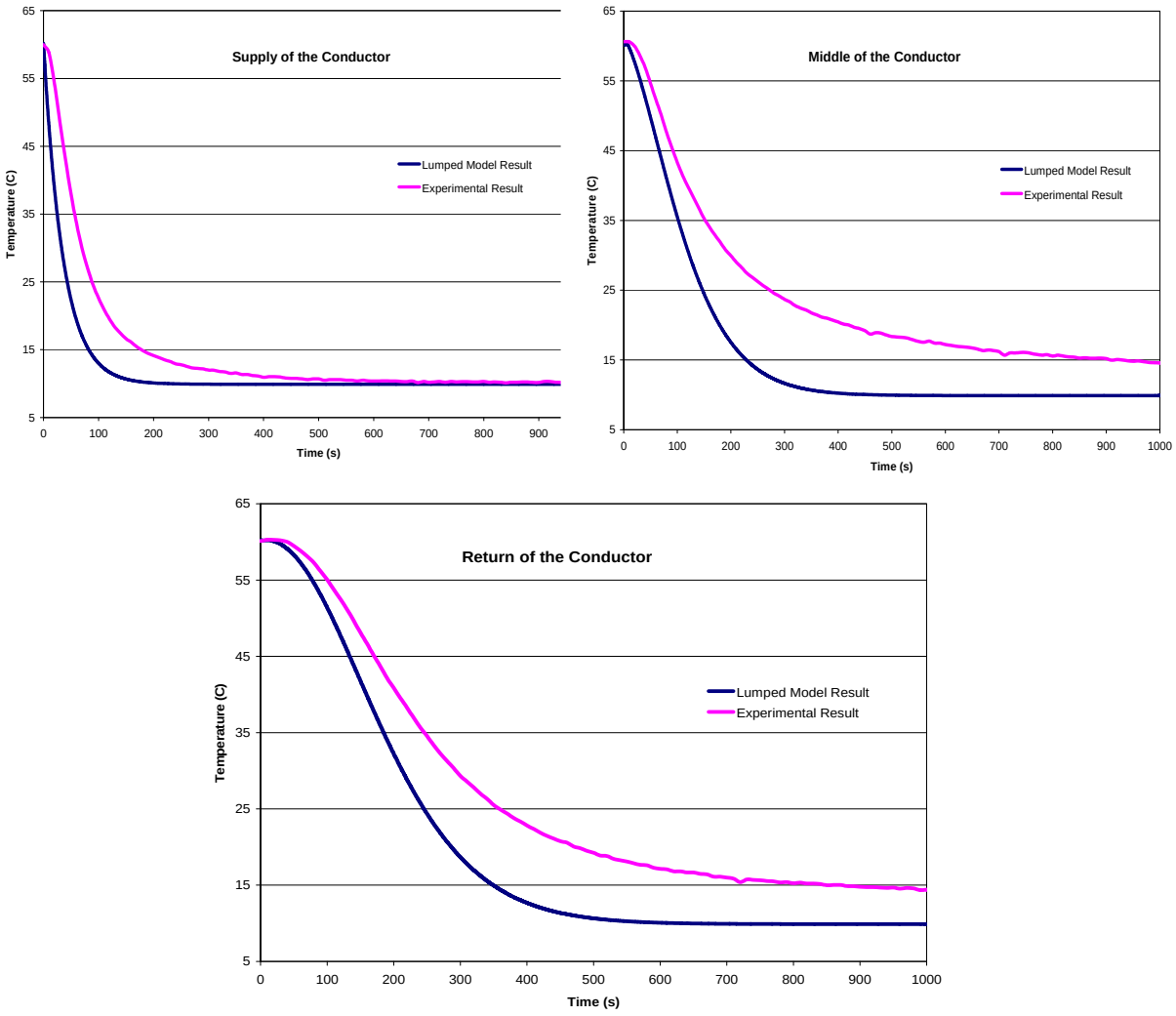

Figure 5.5 Comparisons between experimental and predicted cooling curves (at the supply, middle, and return of the conductor length) for the lumped model with axial conduction when 12.2m long conductor was cooled by 9.9°C water flowing through the through the cooling tube at 0.1GPM. In all predictions, the heat resistance parameter, L*, was 9 mm.

Conductor Length = 12.2 m, Water Flow Rate = 0.15 GPM, Conductor Initial Temperature = 60.9°C, Water Inlet Temperature = 9.8°C, Heat Resistance Parameter = 9 mm

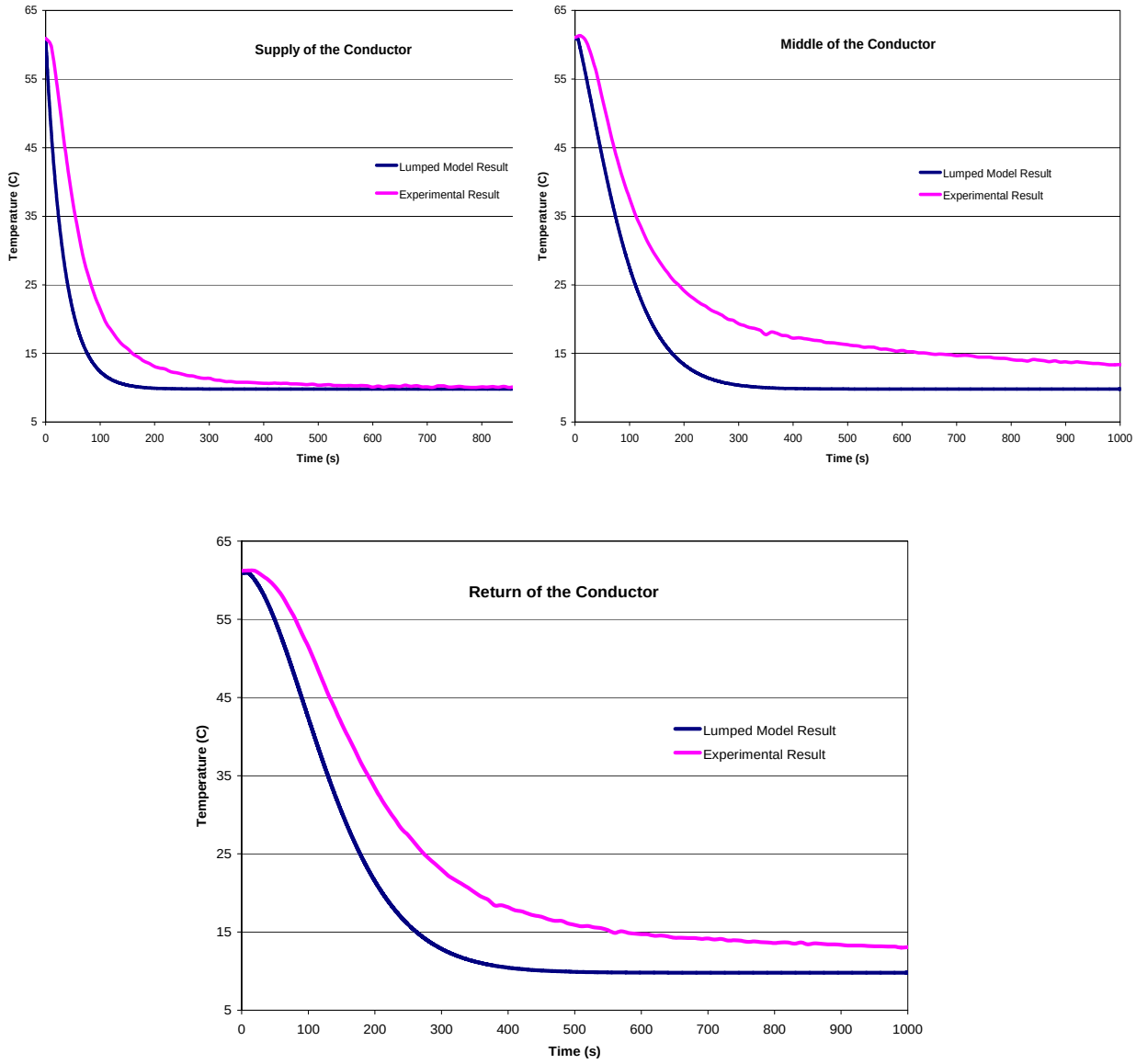

Figure 5.6 Comparisons between experimental and predicted cooling curves (at the supply, middle, and return of the conductor length) for the lumped model with axial conduction when a 12.2m long conductor was cooled by 9.8°C water flowing through the cooling tube at 0.15 GPM. In all predictions, the heat resistance parameter, L*, was 9 mm.

Conductor Length = 12.2 m, Water Flow Rate = 0.2 GPM, Conductor Initial Temperature = 60.9°C, Water Inlet Temperature = 9.1°C, Heat Resistance Parameter = 9 mm

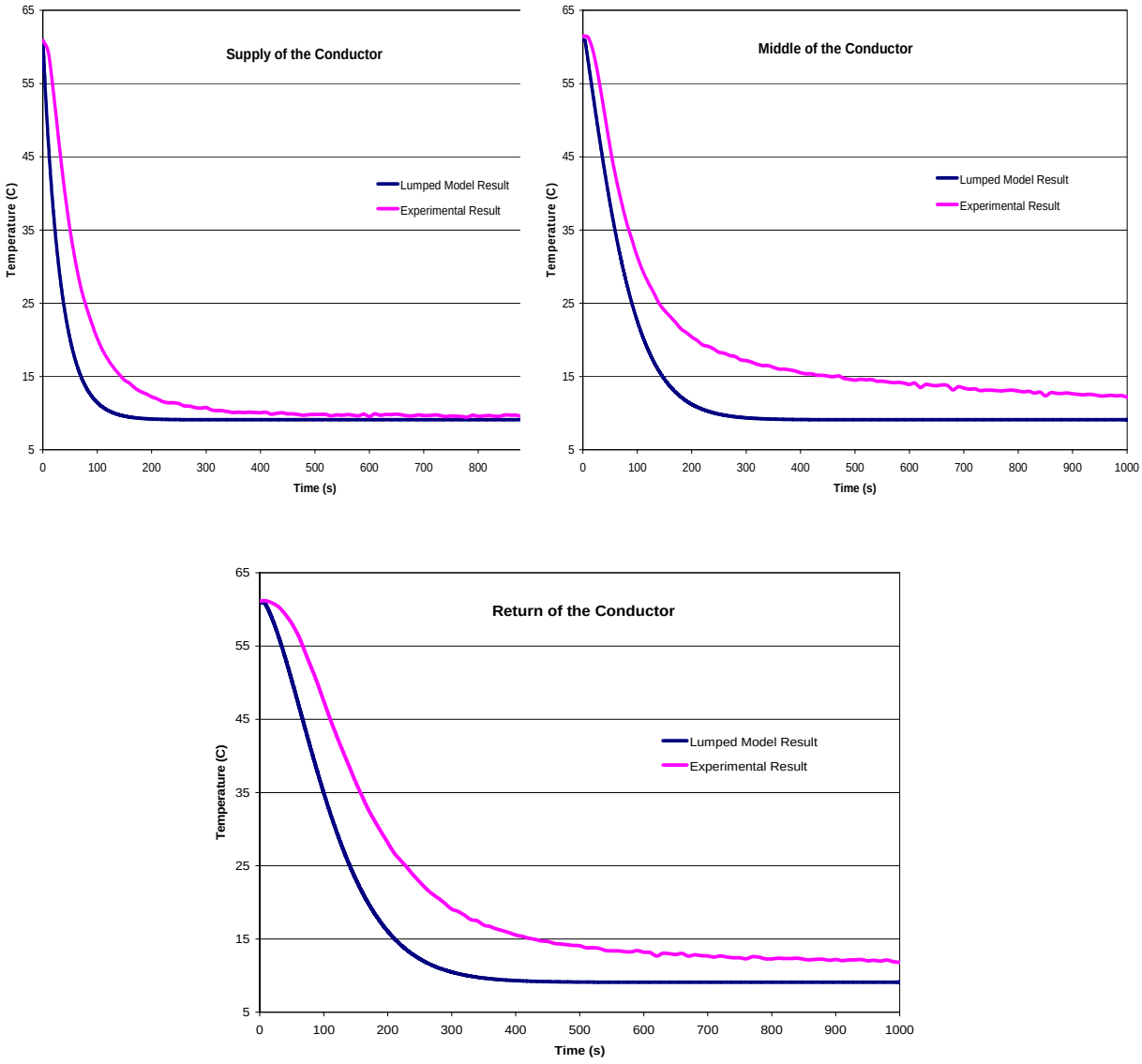

Figure 5.7 Comparisons between experimental and predicted cooling curves (at the supply, middle, and return of the conductor length) for the lumped model with axial conduction when a 12.2m long conductor was cooled by 9.1°C water flowing through the cooling tube at 0.2 GPM. In all predictions, the heat resistance parameter, L*, was 9 mm.

Conductor Length = 12.2 m, Water Flow Rate = 0.25 GPM, Conductor Initial Temperature = 60.5°C, Water Inlet Temperature = 9.4°C, Heat Resistance Parameter = 9 mm

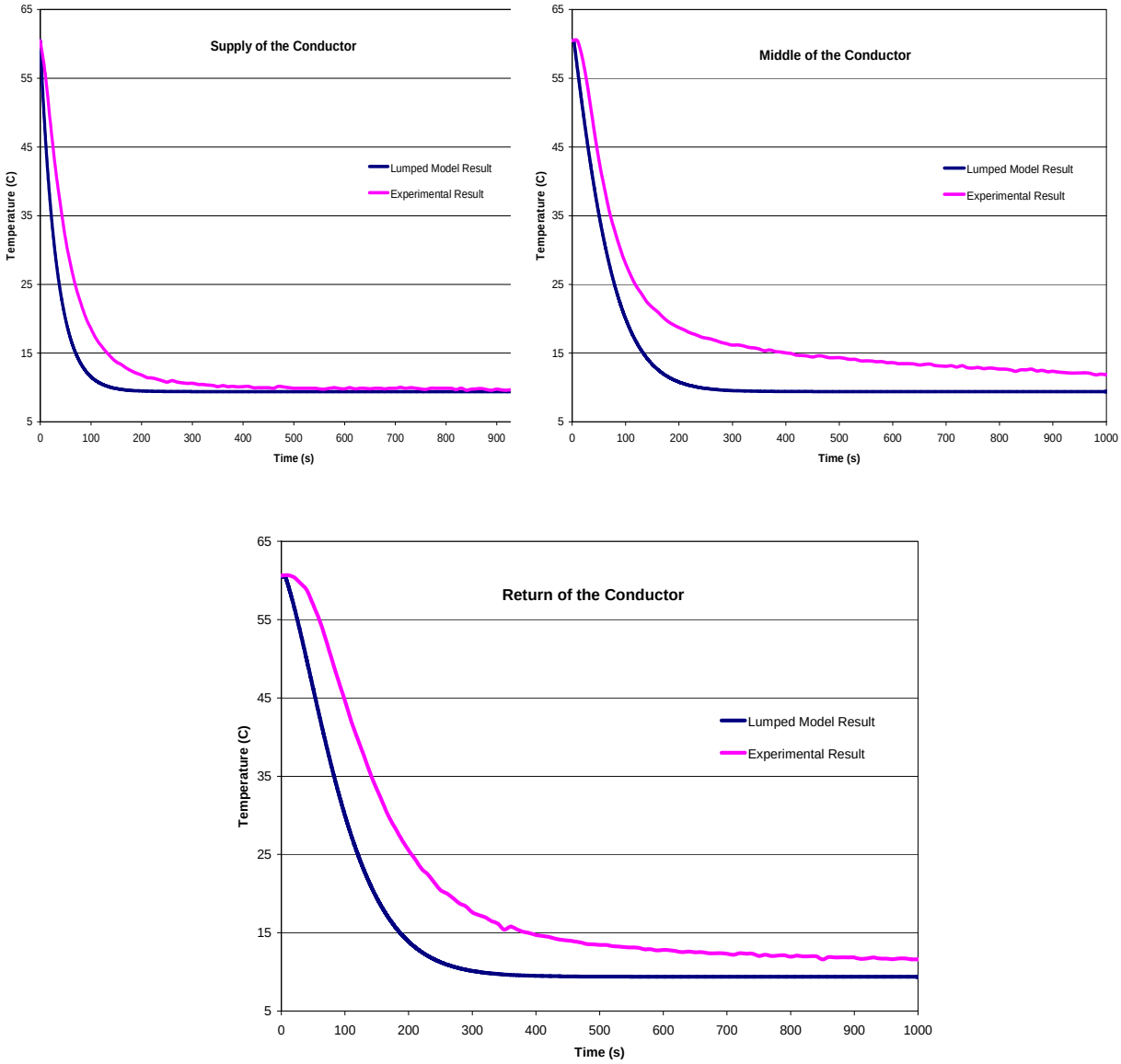

Figure 5.8 Comparisons between experimental and predicted cooling curves (at the supply, middle, and return of the conductor length) for the lumped model with axial conduction when a 12.2m long conductor was cooled by 9.4°C water flowing through the cooling tube at 0.25 GPM. In all predictions, the heat resistance parameter, L*, was 9 mm.

Conductor Length = 12.2 m, Water Flow Rate = 0.3 GPM, Conductor Initial Temperature = 62.7°C, Water Inlet Temperature = 9.5°C, Heat Resistance Parameter = 9 mm

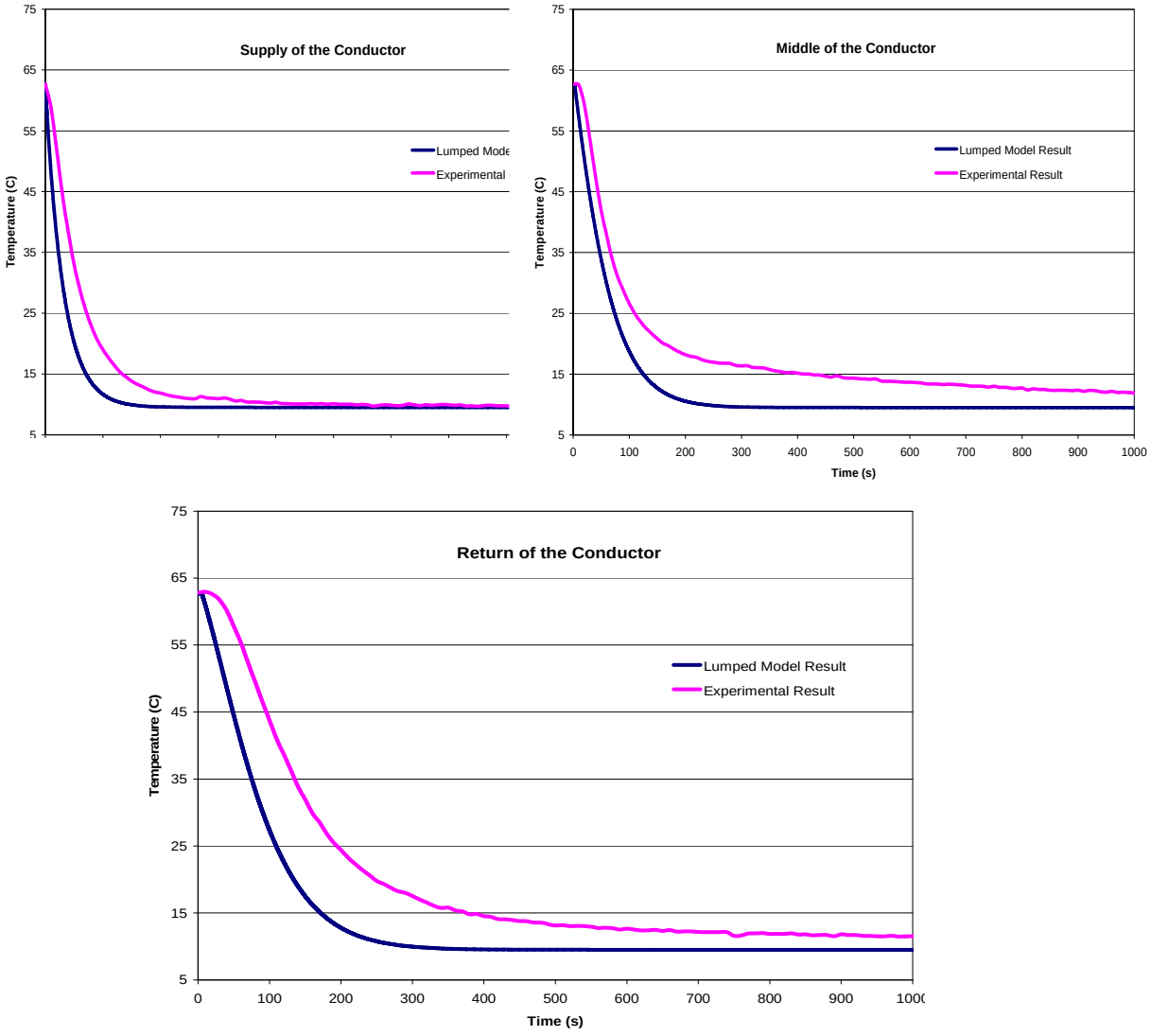

Figure 5.9 Comparisons between experimental and predicted cooling curves (at the supply, middle, and return of the conductor length) for the lumped model with axial conduction when a 12.2m long conductor was cooled by 9.5°C water flowing through the cooling tube at 0.3 GPM. In all predictions, the heat resistance parameter, L*, was 9 mm.

Conductor Length = 12.2 m, Water Flow Rate = 0.1 GPM, Conductor Initial Temperature = 78.9°C, Water Inlet Temperature = 10°C, Heat Resistance Parameter = 9 mm

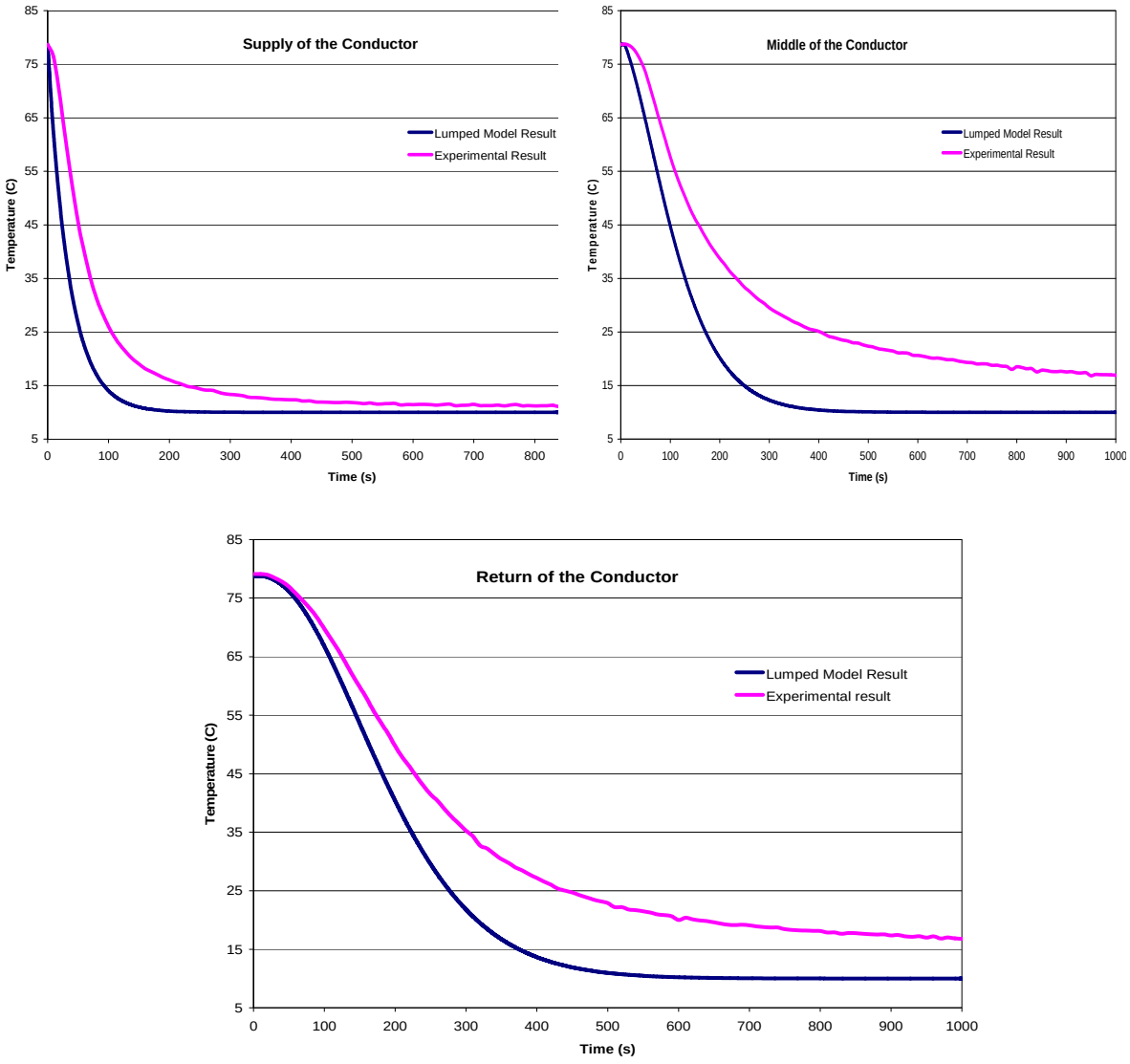

Figure 5.10 Comparisons between experimental and predicted cooling curves (at the supply, middle, and return of the conductor length) for the lumped model with axial conduction when a 12.2m long conductor was cooled by 10°C water flowing through the cooling tube at 0.1 GPM. In all predictions, the heat resistance parameter, L*, was 9 mm.

Conductor Length = 12.2 m, Water Flow Rate = 0.15 GPM, Conductor Initial Temperature = 78.8°C, Water Inlet Temperature = 9.8°C, Heat Resistance Parameter

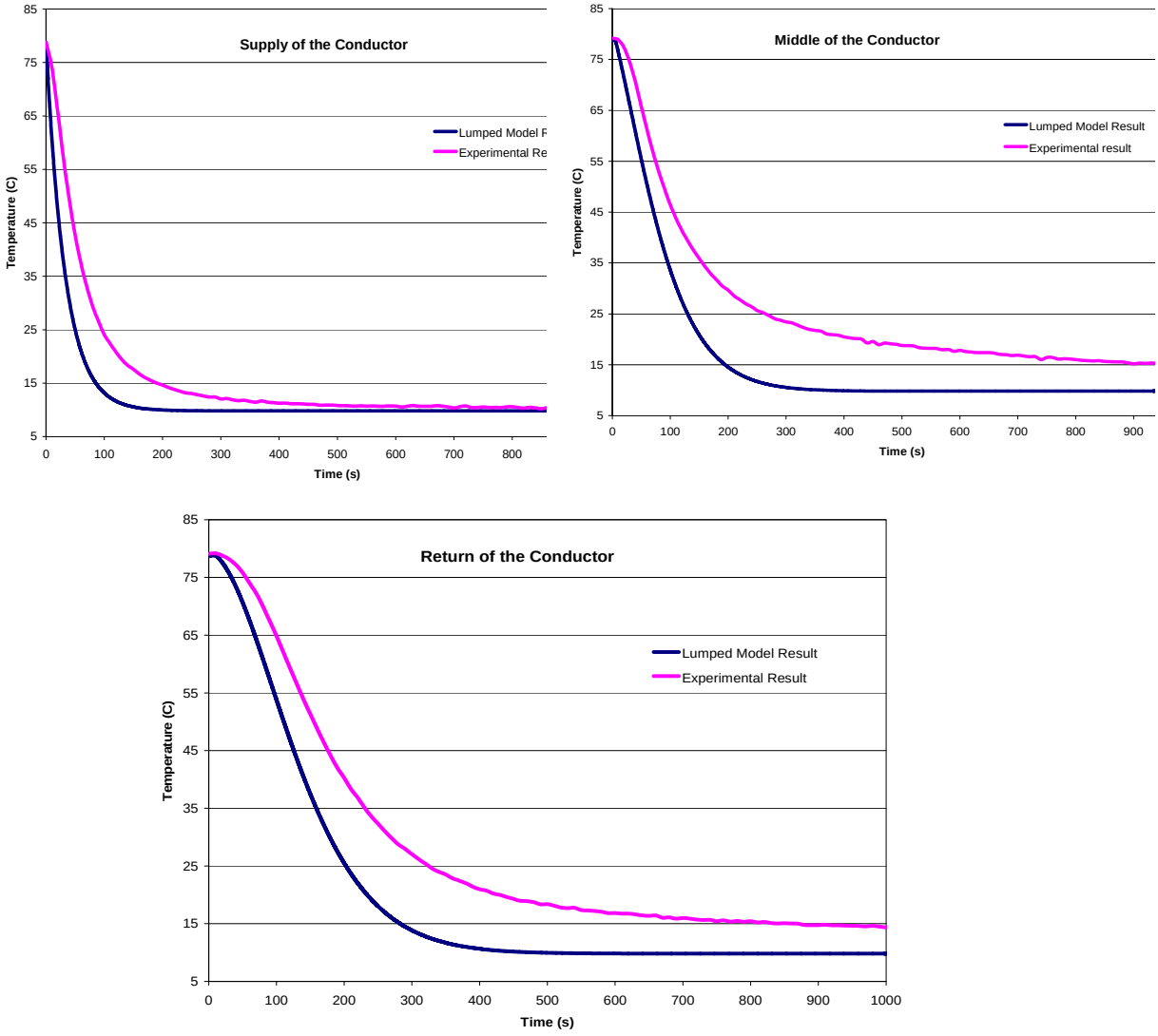

Figure 5.11 Comparisons between experimental and predicted cooling curves (at the supply, middle, and return of the conductor length) for the lumped model with axial conduction when a 12.2m long conductor was cooled by 9.8°C water flowing through the cooling tube at 0.15 GPM. In all predictions, the heat resistance parameter, L*, was 9 mm.

Conductor Length = 12.2 m, Water Flow Rate = 0.2 GPM, Conductor Initial Temperature = 76.4°C, Water Inlet Temperature = 10°C, Heat Resistance Parameter = 9 mm

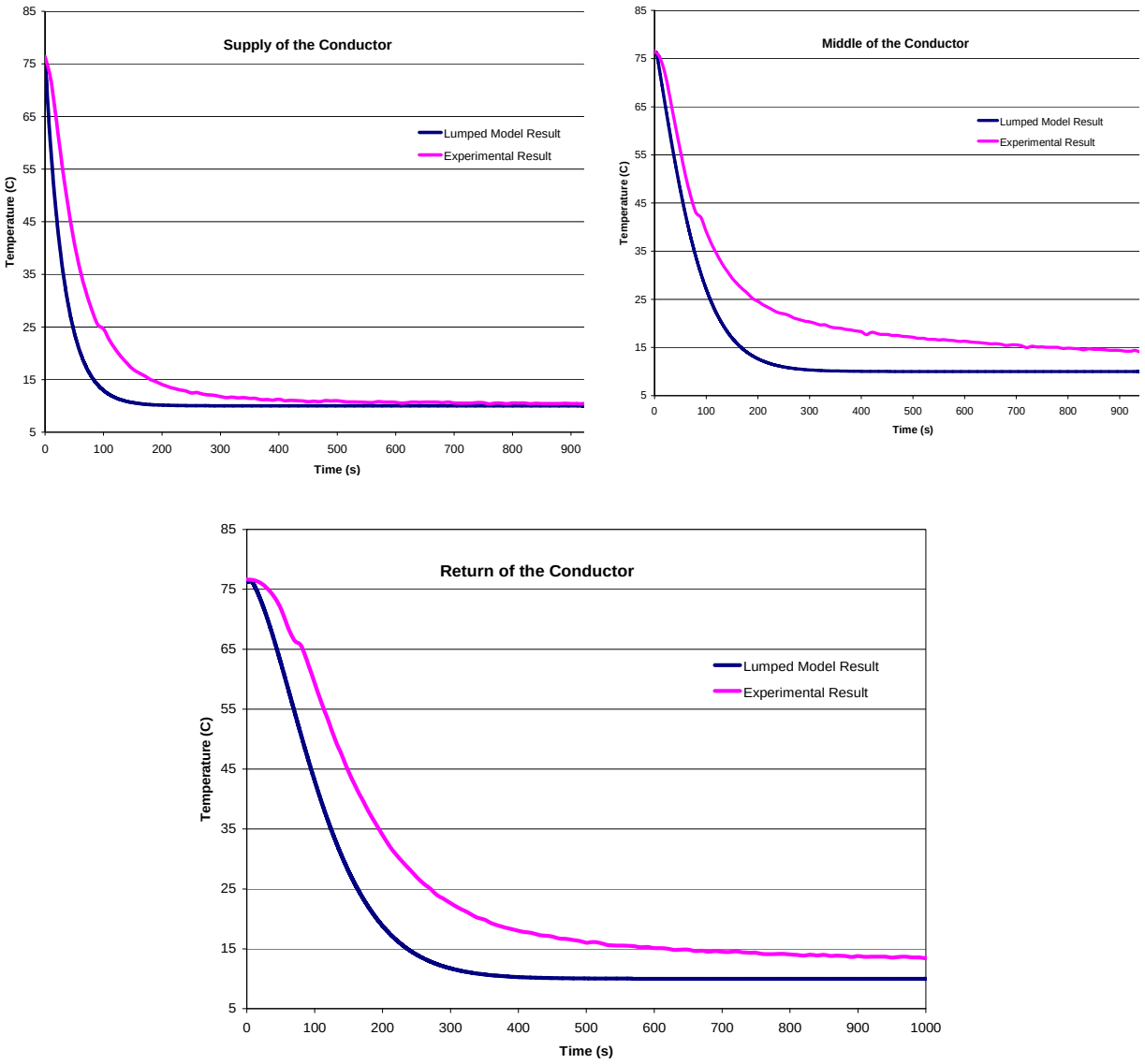

Figure 5.12 Comparisons between experimental and predicted cooling curves (at the supply, middle, and return of the conductor length) for the lumped model with axial conduction when a 12.2m long conductor was cooled by 10°C water flowing through the cooling tube at 0.2 GPM. In all predictions, the heat resistance parameter, L*, was 9 mm.

Conductor Length = 12.2 m, Water Flow Rate = 0.25 GPM, Conductor Initial Temperature = 79.3°C, Water Inlet Temperature = 10.3°C, Heat Resistance Parameter = 9 mm

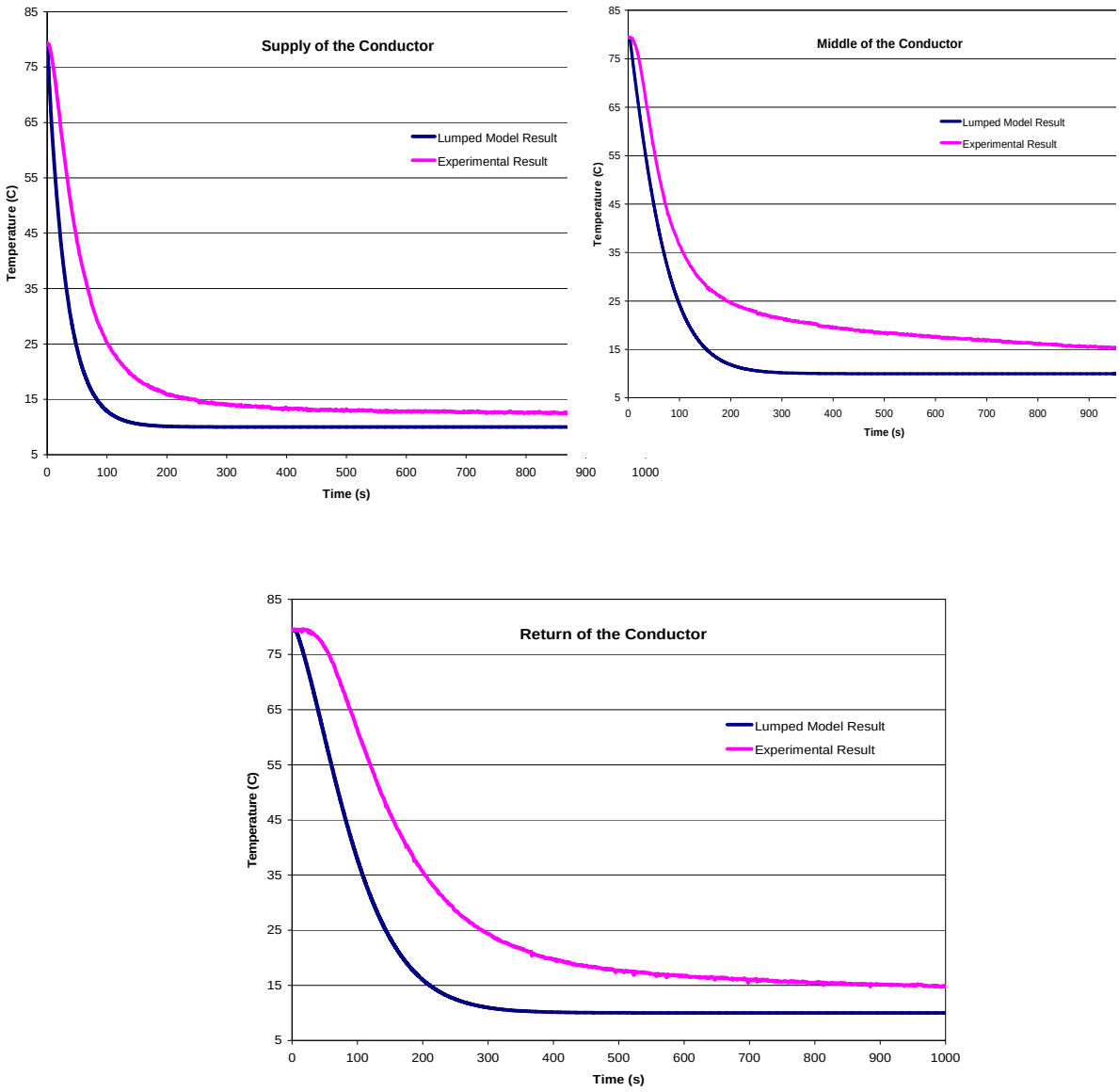

Figure 5.13 Comparisons between experimental and predicted cooling curves (at the supply, middle, and return of the conductor length) for the lumped model with axial conduction when a 12.2m long conductor was cooled by 10.3°C water flowing through the cooling tube at 0.25 GPM. In all predictions, the heat resistance parameter, L*, was 9 mm.

Conductor Length = 12.2 m, Water Flow Rate = 0.3 GPM, Conductor Initial Temperature = 76.1°C, Water Inlet Temperature = 9.6°C, Heat Resistance Parameter = 9 mm

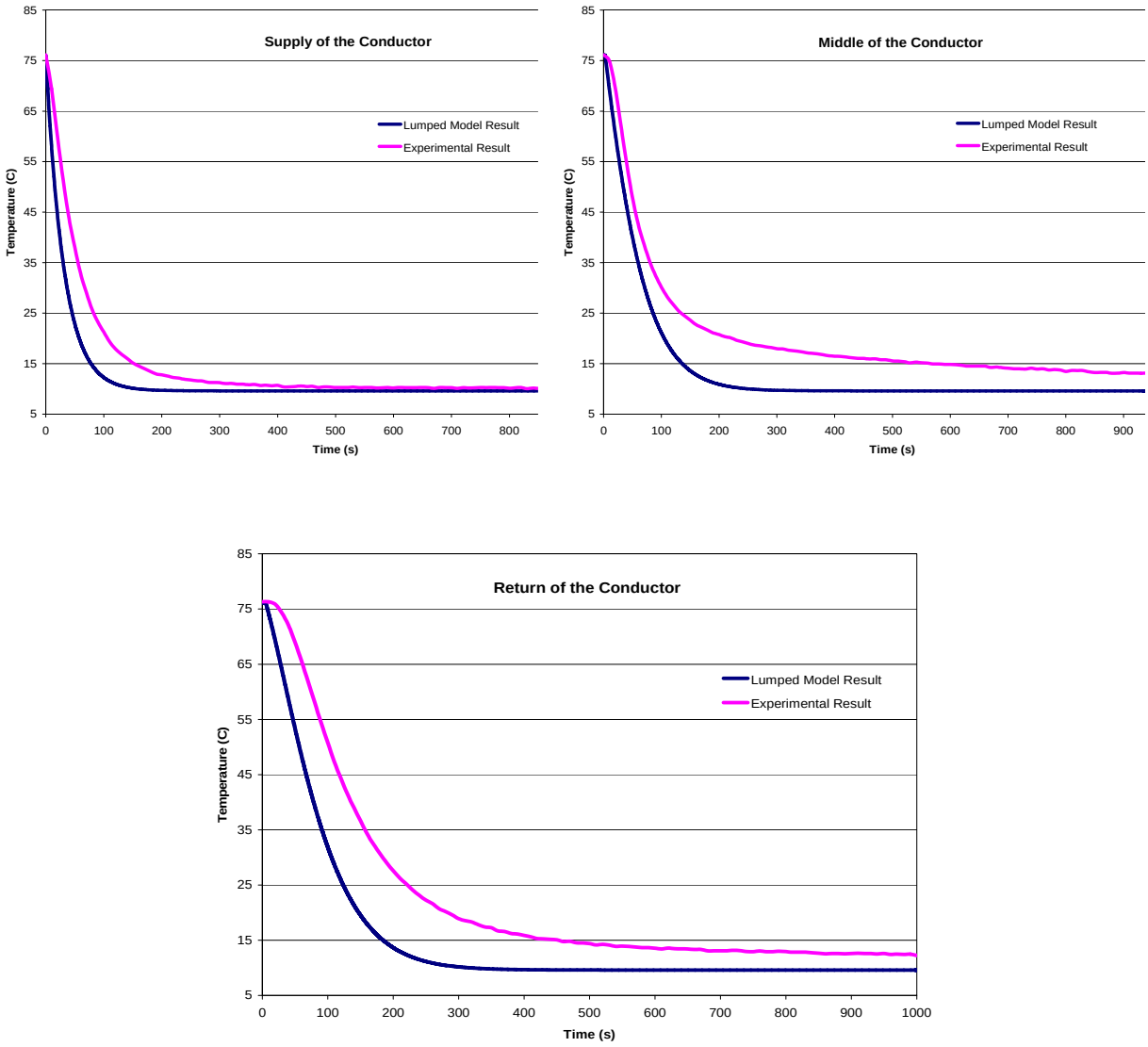

Figure 5.14 Comparisons between experimental and predicted cooling curves (at the supply, middle, and return of the conductor length) for the lumped model with axial conduction when a 12.2m long conductor was cooled by 9.6°C water flowing through the cooling tube at 0.3 GPM. In all predictions, the heat resistance parameter, L*, was 9 mm.

From the typical heating and cooling graph in Figure 3.12 in Chapter 3, the conductor pie 1 was seen to be clearly heating at a faster rate than the conductor pie 3. This was due to the presence of large metal mass (heat sink) closer to conductor pie 1 than it was to pie 3. The temperatures were expected to become almost the same after some amount of time but even after about 20 hours of heating, the conductor pie 3 never reached the temperature of pie 1. This suggested that there was a continuous leakage through the oven and that they would not cool at the same rate during the cooling process. The cooling process proved this.

Also, as can be seen from the graphs that for both cases (cooling from 60°C and from 80°C), there is a poor agreement between experiment and predictions. The LMAC predictions do not match the recorded cooling data at the conductor inlet. The difference between the experiment and predictions is larger at points farther away (i.e. at the middle and the end of the conductor) from the inlet. In these cases, the lumped model was seen to cool faster than the experiment. The following reasons are believed to be responsible for the poor agreement between experiments and predictions at points away from the conductor inlet:

1. As explained earlier in Chapter 3, due to the pie arrangement of the conductors, conductor pie 2 was sandwiched between pie 1 and pie 3. Pie 1was in contact with the large steel mass (wall of the winding form). As a result of this, it was absorbing heat from the winding form throughout the cooling process, making the cooling rate of pie 1 slower than if it was not adjacent to the winding form. Similarly pie 3 was adjacent to coils which were not cooled by cooling water. As a result the temperature of pie 3 was also higher than pie 2 which contributed to slowing of the cooling rate of pie 2 conductor. One way to produce the cooling rate of pie 1 and pie 3 to be same as that of pie 2 may have been to send water through pie 1 and pie 3 at a higher flow rate than pie 2. However, the difficulty would lie in knowing the correct flow rate to use. Such attempts are left for future research.

2. Another source of the erroneous data is believed to be the fact that since the conductor is wrapped around a cylindrical form, there is a "cross-talk" within each conductor, i.e. there will also be heat transfer between adjacent layers within the same conductor as shown in Figure 5.15. The model used here did not account for such "cross-talk." Modification of the model to incorporate the heat transfer among the adjacent layers is part of the future research.

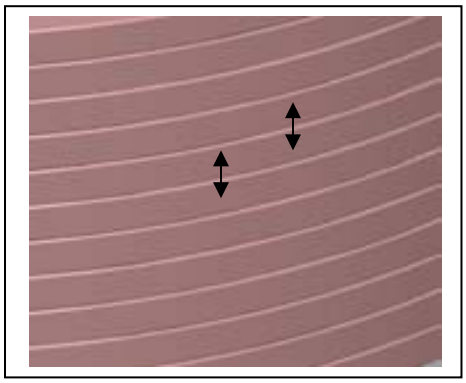

Figure 5.15 A section of conductor winding showing the possibility of heat transfer between adjacent layers.

6. CONCLUSIONS

This research addressed two issues:

1) Modification of the radially lumped model to account for the axial heat transfer, and
2) Testing the applicability of the modified model to predict the cooling behavior of 5.5 m long and 12.2 m long conductors.

The first issue was successfully implemented in this research. The modified model provides a simple engineering tool to account for heat transfer both in the radial and the axial directions. By comparing the model predictions for very low flow rates (0.005 GPM) with that for the larger flow rates (larger than 0.1 GPM), it was demonstrated that for the flow rates expected in the QPS coils (larger than 0.1 GPM), the axial heat transfer can be neglected. In such cases, the analysis that includes only the radial heat transfer will suffice.

While the experimental data for the cooling of 5.5 m long conductor was taken from literature, the experimental data on 12.2 m long conductor was generated during this research. Several lessons were learnt both in regard to the vacuum impregnation of the long circular conductor as well as on the experiments on heat transfer of these conductors. These are listed below:

a) The oven used was too small for both the vacuum pressure impregnation and the heating/cooling experiments of the large conductor used in this study. Because of the small sized oven, the heating elements were too close to the conductor at several locations producing a non uniform heating of the conductor.
b) The open ends of the cooling tube were not properly sealed, which resulted in the suction of the liquid resin into the tubes during the vacuum application. As a result the 25 m long conductor tube could not be used.
c) In spite of the ample use of the glass-fiber insulation material on all exposed surfaces of the conductor, there was still (non uniform) heat loss through the conductor. This prevented the entire conductor to reach one temperature in spite of the long heating time of 20 hours.

d) With the presence of the large metal mass of the winding form, the conductor layers in direct contact with the form did not cool at the same rate as the ones which were not in direct contact. In addition, since the adjacent layers of the same conductor were in direct contact, there was additional temperature adjustment within each conductor. As a result, the conditions assumed in the lumped model could not be reproduced in the experiments.

7. FUTURE WORK

Based on the lessons learnt, the following recommendations are made for the future work:

1) A larger and well-insulated oven should be used to conduct the heating/cooling experiments.
2) Since manufacturing the conductor took the majority of the time of this research, we suggest that additional experiments should be conducted on the same conductor to improve the quality of the experimental data. For example, the flow rates in pie 1 and pie 3 should be changed until all three conductors (pie 1, pie 2, and pie 3) yield the same cooling curves.
3) It is believed that if the steel form can be removed from the windings, a better quality cooling data will be obtained.
4) The lumped model should be modified to account for the heat transfer between the adjacent layers of the same conductor. This can be done by adding another routine in the code at each time step. Such a routine will use the similar equations that were used for the axial heat transfer.
5) Only after these issues are addressed, can the validity of the lumped model for predicting the cooling behavior of long conductors be assessed.

REFERENCES

1. Evans, Robert L. Fueling Our Future: An Introduction to Sustainable Energy. New York: Cambridge UP, 2007. pp. 6,7,115.
2. Energy Information Administration, International Energy Outlook. 2008. World Energy Demand and Economic Outlook. http://www.eia.doe.gov/oiaf/ieo/pdf/world.pdf. Accessed: December 11, 2008.
3. Kursunoglu, Behram N., Andrew C. Millunzi, and Arnold Perlmutter, eds. A Global View of Energy. New York: Free P, 1982. pp. 44,45.
4. McVeigh, J. C. Energy Around the World : An Introduction to Energy Studies: Global Resources, Needs, Utilization. New York: Pergamon, 1984. p.148.
5. Hedley, D. World Energy, the Facts and the Future. Euromonitor Publications Limited (Oxford), England, 1981. p.188.
6. Nuttal, W. J. Fusion as an Energy Source: Challenges and Opportunities. London, UK: Institute of Physics, 2008. http://ioppublishing.com/activity/policy/Publications/file_31695.pdf. Accessed: December 10, 2008.
7. LAP (Associated Plasma Laboratory). Tokamaks. http://www.plasma.inpe.br/LAP_Portal/LAP_Site/Text/Tokamaks.htm. Accessed: March 14, 2009.
8. Wikipedia. 2009. Tokamak. http://en.wikipedia.org/wiki/Tokamak. Accessed: March 14, 2009.
9. Chaudhri, A., P. Masood, and B. E. Nelson. "Thermal modeling and analysis of a thermal modeling and analysis of a quasi-poloidal stellarator modular coil." Applied Thermal Engineering 26 (2006): 974-82.
10. Freudenberg, K. D., P. Goranson and F. Dahlgren, Cooling design and analysis of the QPS modular coil winding packs, 21st IEEE/NPPS Symposium on Fusion Engineering, 2005.

11. Kandala, B. Numerical Simulation (A Lumped Transient Model) for QPS Modular Coils with embedded Copper Tubes and subsequent Experimental verification". MS Thesis, December (2008), University of Tennessee, Knoxville.
12. Narasimhaswami, S. Cooling of QPS Modular Coils Using Embedded Copper Tubes. MS Thesis, December (2006), University of Tennessee, Knoxville.
13. Sun, Y., and I. S. Wichman. "On transient heat conduction in one-dimensional composite slab." International Journal of Heat and Mass Transfer 47 (2004): 1555-559.
14. Salt, H. "Transient conduction in a two-dimensional composite slab-I. Theoretical development of temperature modes." International Journal of Heat and Mass Transfer 26 (1983): 1611-616.
15. Monte, F. De. "A 'natural' analytical approach to transient heat conduction in one-dimensional composite slab." International Journal of Heat and Mass Transfer 43 (2000): 3607-619.
16. Chopra, M. G., and I. J. Marwah. "Transient Heat Transfer in Composite Solids with Non-Linear Boundary Condition." Def Sci J 40 (1990): 275-82.
17. Bilir, S. and A. Ates. "Transient conjugated heat transfer in thick walled pipes with convective boundary conditions." International Journal of Heat and Mass Transfer 46 (2003): 2701-709.
18. Loh, J. S., I. A. Azid, K. N. Seetharamu, and G. A. Quadir. "Fast transient thermal analysis of Fourier and non-Fourier heat conduction." International Journal of Heat and Mass Transfer 50 (2007): 4400-408.
19. Corlay, C., and S. G. Advani. "Temperature distribution in a thin composite plate exposed to a concentrated heat source." International Journal of Heat and Mass Transfer 50 (2007): 2883-894.
20. Hong-Liang, Y., M. Xie, and T. He-Ping. "Transient coupled heat transfer in an anisotropic scattering composite slab with semitransparent surfaces." International Journal of Heat and Mass Transfer 51 (2008): 5918-930.

21. Haji-Sheikh, A., D. E. Amos, and J. V. Beck. "Axial heat conduction in a moving semi-infinite fluid." International Journal of Heat and Mass Transfer 51 (2008): 4651-658.
22. Beck, J. V., N. T. Wright, A. Haji-Sheikh, K. D. Cole, and D. E. Amos. "Conduction in rectangular plates with boundary temperatures specified." International Journal of Heat and Mass Transfer 51 (2008): 4676-690.
23. Gordeliy, E., S. L. Crouch, and S. G. Mogilevskaya. "Transient heat conduction in a medium with two circular cavities: semi-analytical solution." International Journal of Heat and Mass Transfer 51 (2008): 3556-570.
24. Pitts, D. R. Schaum's outline of theory and problems of heat transfer. New York: McGraw-Hill, 1998. p. 190.
25. Myers, Glen E. Analytical methods in conduction heat transfer. Schenectady, NY: Genium Pub. Corp., 1987.pp. 103-112.
26. Chin-Chi T., B. E. Nelson, and H. Wang, Thermal Diffusivity Measurements of Monolithic Copper-Epoxy Composite Specimens by the Flash Method. 27th International Thermal Conductivity Conference (ITCC27) and the 15th International Thermal Expansion Symposium (ITES15), Ed. H. Wang and W.D. Porter, (2006) pp. 413-423.

APPENDICES

Appendix A

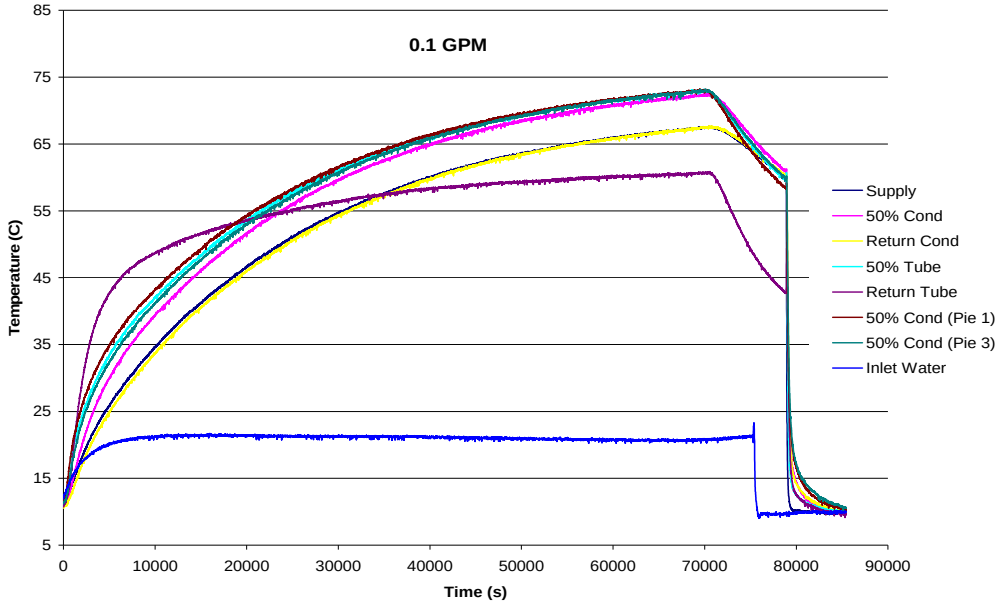
0.1 GPM
Temperature (C)
Time (s)
85
75
65
55
45
35
25
15
5
0
10000
20000
30000
40000
50000
60000
70000
80000
90000
Supply
50% Cond
Return Cond
50% Tube
Return Tube
50% Cond (Pie 1)
50% Cond (Pie 3)
Inlet Water

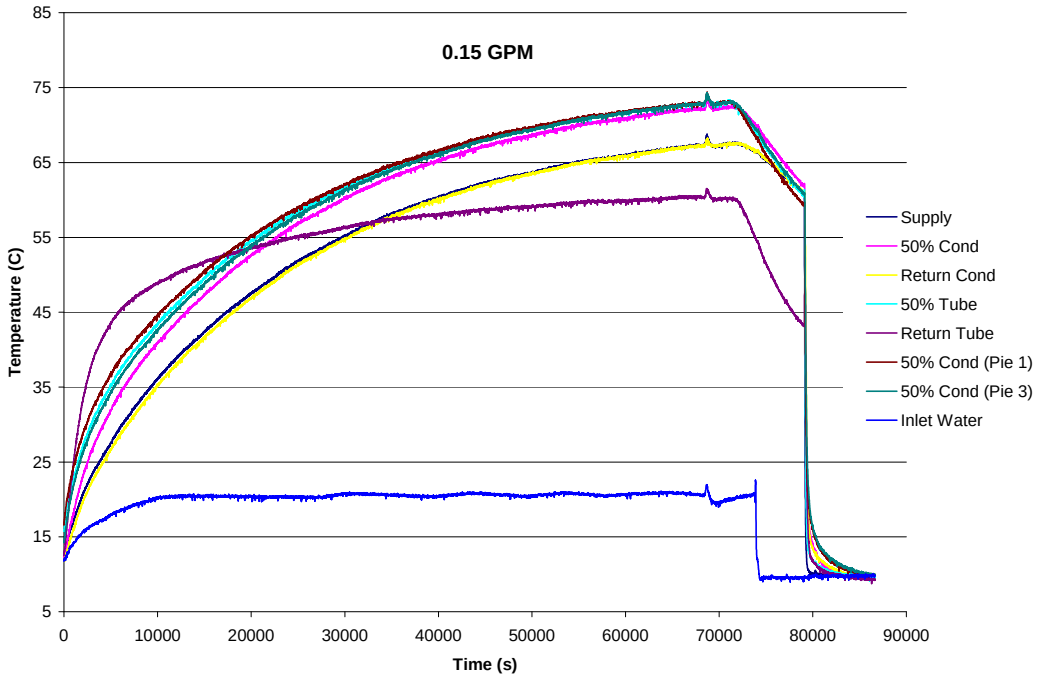
0.15 GPM
Temperature (C)
Time (s)
85
75
65
55
45
35
25
15
5
0
10000
20000
30000
40000
50000
60000
70000
80000
90000
Supply
50% Cond
Return Cond
50% Tube
Return Tube
50% Cond (Pie 1)
50% Cond (Pie 3)
Inlet Water

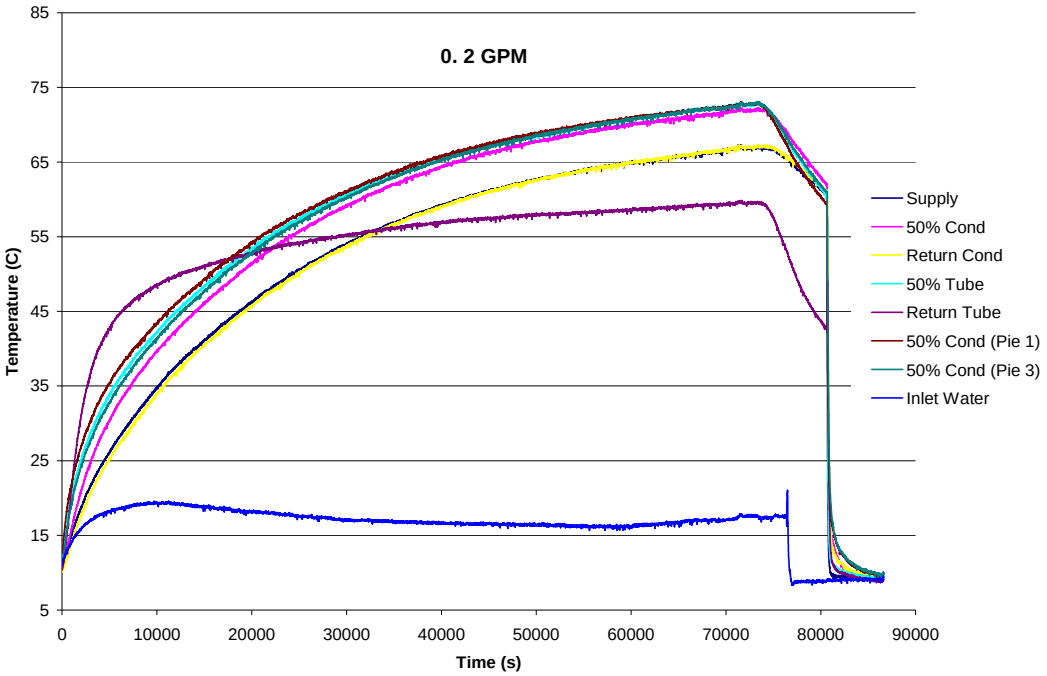
0. 2 GPM
Temperature (C)
Time (s)
85
75
65
55
45
35
25
15
5
0
10000
20000
30000
40000
50000
60000
70000
80000
90000
Supply
50% Cond
Return Cond
50% Tube
Return Tube
50% Cond (Pie 1)
50% Cond (Pie 3)
Inlet Water

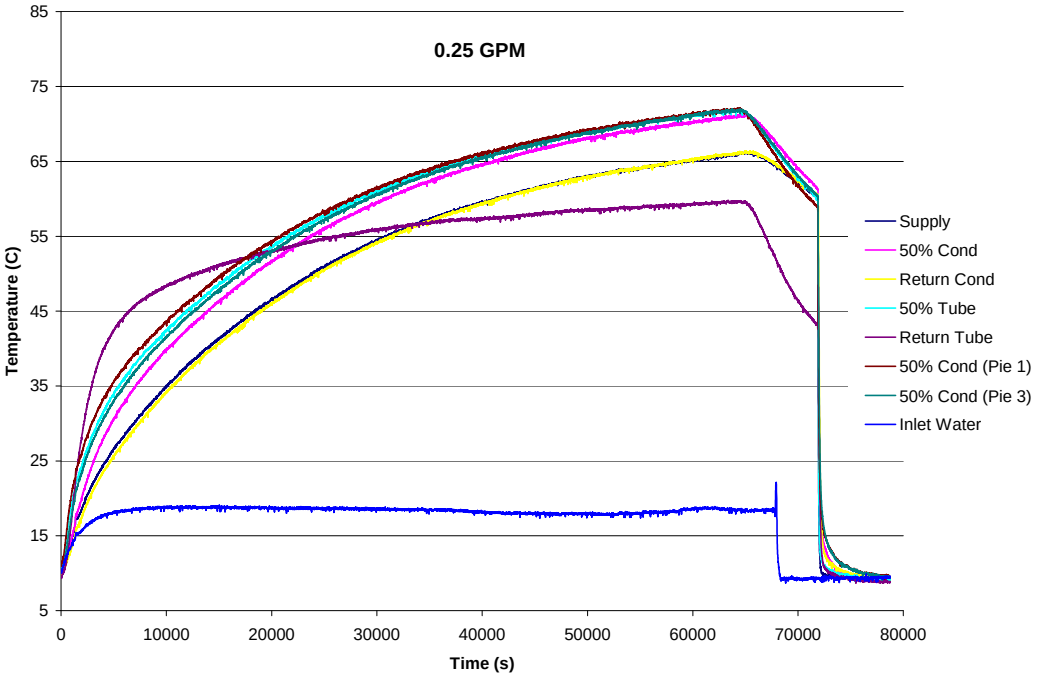
0.25 GPM
Temperature (C)
Time (s)
85
75
65
55
45
35
25
15
5
0
10000
20000
30000
40000
50000
60000
70000
80000
Supply
50% Cond
Return Cond
50% Tube
Return Tube
50% Cond (Pie 1)
50% Cond (Pie 3)
Inlet Water

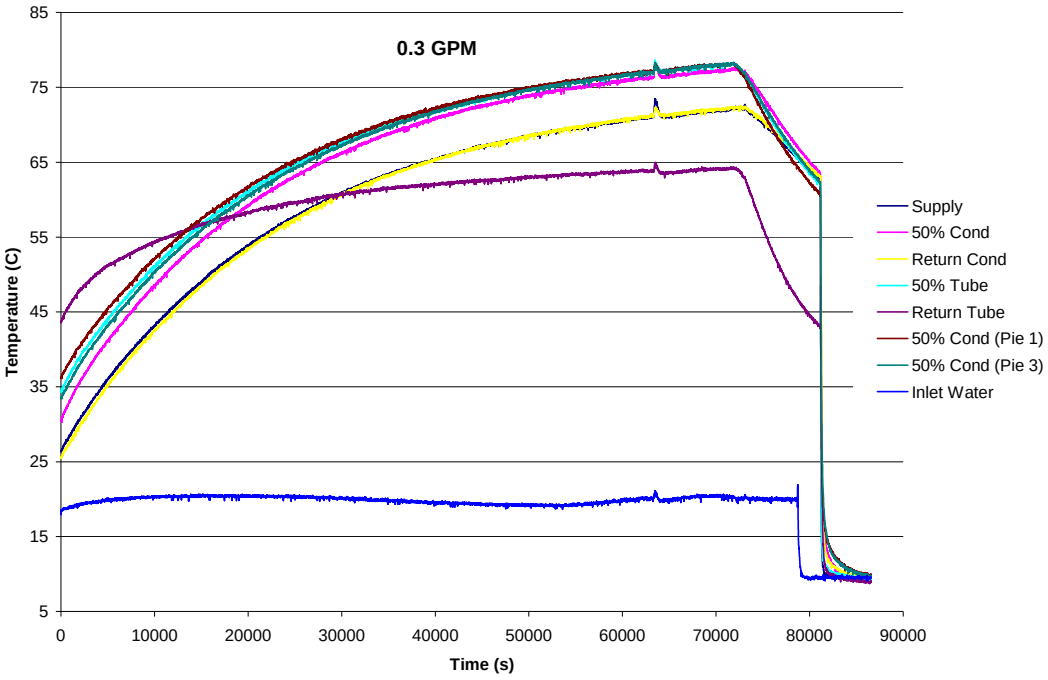

Experimental results for all flow rates of 0.1, 0.15. 0.2, 0.25, and 0.3 GPM when the 12.2 m long conductor was cooled from approximately

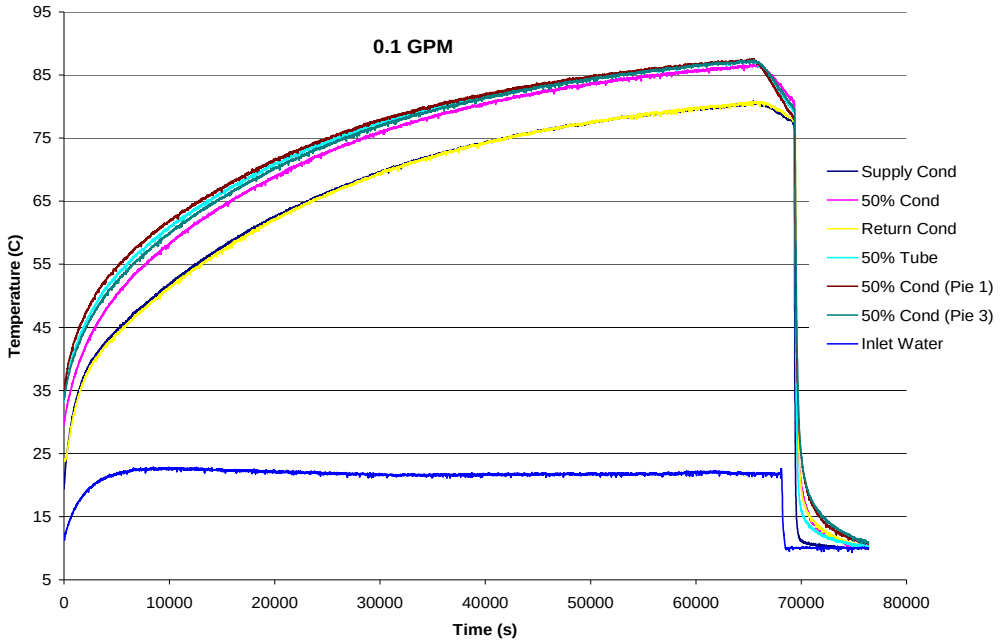
0.1 GPM
Temperature (C)
Time (s)
95
85
75
65
55
45
35
25
15
5
0
10000
20000
30000
40000
50000
60000
70000
80000
Supply Cond
50% Cond
Return Cond
50% Tube
50% Cond (Pie 1)
50% Cond (Pie 3)
Inlet Water

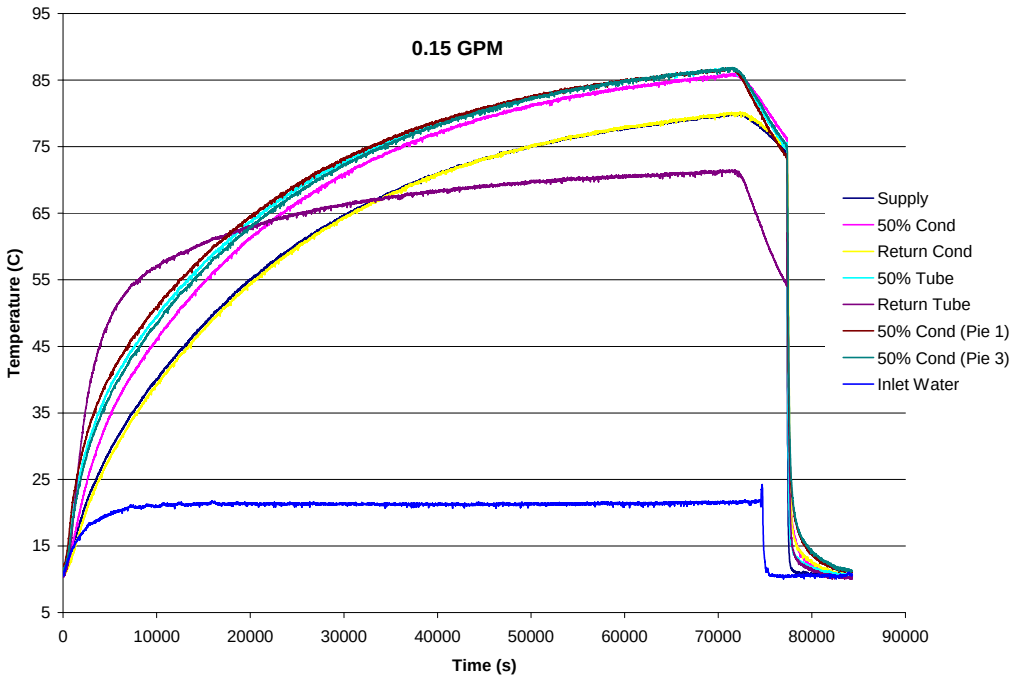
0.15 GPM
Temperature (C)
Time (s)
95
85
75
65
55
45
35
25
15
5
0
10000
20000
30000
40000
50000
60000
70000
80000
90000
Supply
50% Cond
Return Cond
50% Tube
Return Tube
50% Cond (Pie 1)
50% Cond (Pie 3)
Inlet Water

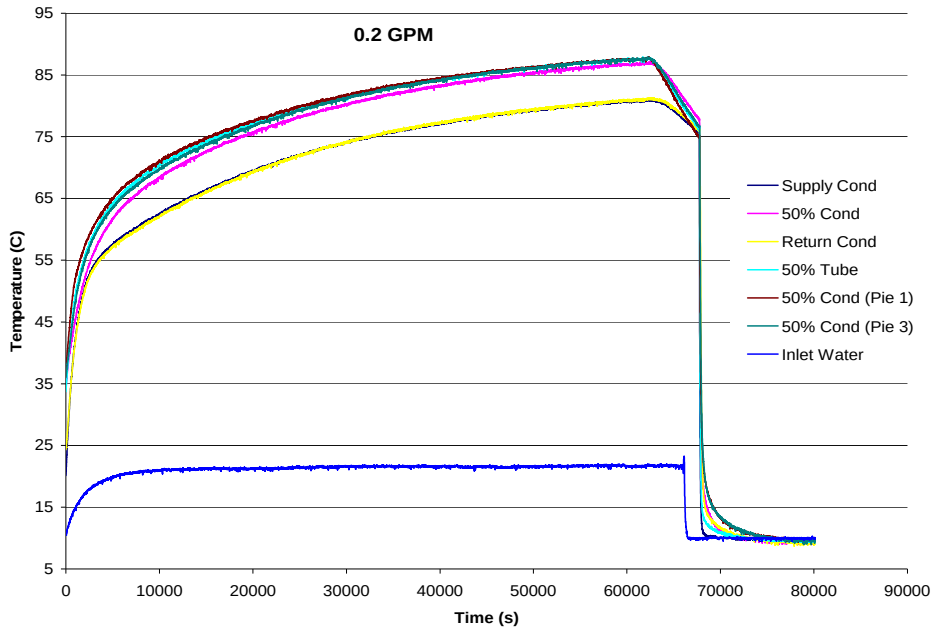
0.2 GPM
Temperature (C)
Time (s)
95
85
75
65
55
45
35
25
15
5
0
10000
20000
30000
40000
50000
60000
70000
80000
90000
Supply Cond
50% Cond
Return Cond
50% Tube
50% Cond (Pie 1)
50% Cond (Pie 3)
Inlet Water

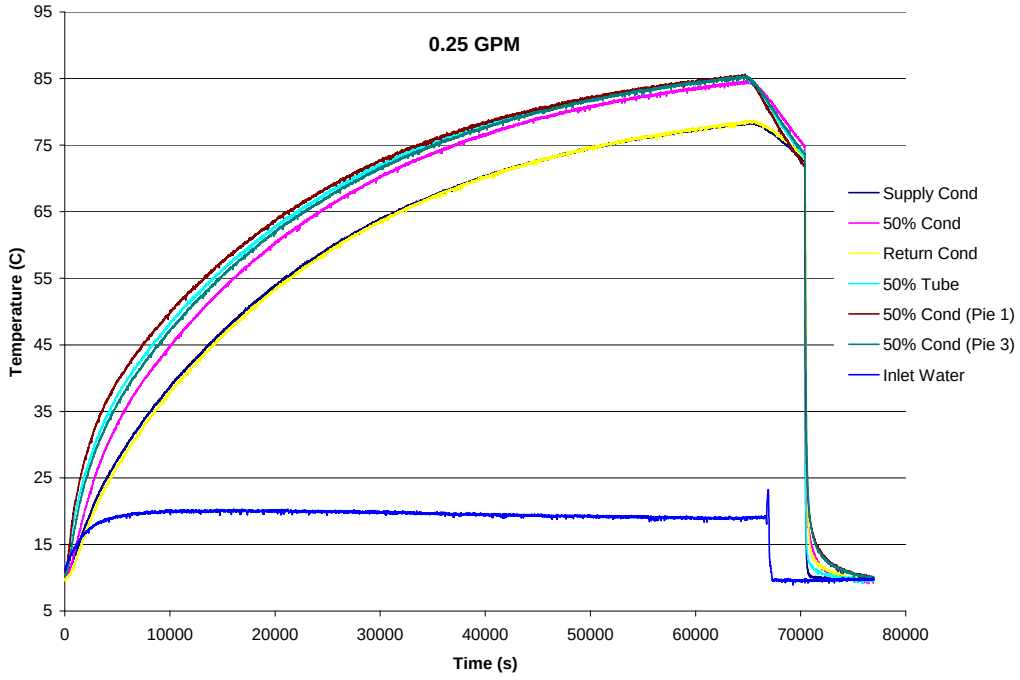
0.25 GPM
Temperature (C)
Time (s)
95
85
75
65
55
45
35
25
15
5
0
10000
20000
30000
40000
50000
60000
70000
80000
Supply Cond
50% Cond
Return Cond
50% Tube
50% Cond (Pie 1)
50% Cond (Pie 3)
Inlet Water

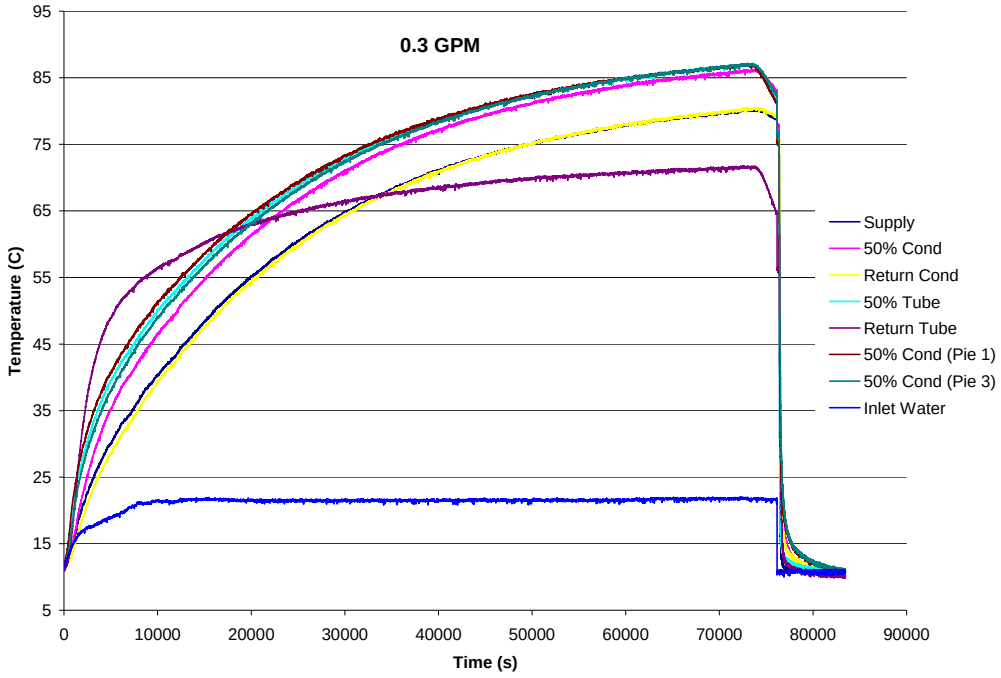

Experimental results for all flow rates of 0.1, 0.15. 0.2, 0.25, and 0.3 GPM when the 12.2 m long conductor was cooled from approximately

Appendix B

```
% HEAT TRANSFER ANALYSIS OF QPS COIL
clc
clear all
% Lumped system analysis
% All units in SI system

% ---- User defined variables ----
Q=0.1; %in gal/min
ri = 0.003239/2; %inside radius in m
A=(pi)*(ri^2); % Cross sectional area in m^2
v= (0.003785412)*(Q)/((A)*(60));% Velocity of water in m/s
length_of_tube = 12.192; % in m
time_of_result = 1000; % result wanted at end of this time period.
n = 1000; % number of elements in the model

  Excel = actxserver('Excel.Application');
              set(Excel, 'Visible', 1);
             % Insert a new workbook
              Workbooks = Excel.Workbooks;
              Workbook = invoke(Workbooks, 'Add');

start_time = cputime ;
% calculation of time step for the given no. of elements
      t_inlet_to_outlet = length_of_tube/v ;
      t = t_inlet_to_outlet/n ;

             % ---- User Print screen data ----
             sprintf ('Length of tube considered = %.2f m.',length_of_tube)
             sprintf ('Velocity of water = %.2f m/s',v)
             sprintf ('Temperature distribution required at time = %.3f
seconds',time_of_result)
             sprintf ('Number of elements used in the model = %.0f ',n)
             sprintf ('Time step used in the model = %.8f ',t)

             % ---- Property Values ---------
             k = 9.9; % Radial Conductivity of Composite 12 W/m-K
             kc = 320; % Axial conductivity of composite in W/m-K
             Tcomposite = 60.18; % Initial temp of Cu composite -- provided later as Tc
             Twater_inlet = 9.91;  % Initial temp of water -- provided later as Tw
%              T_outside = 0; % %Initial temperature of the water
             sprintf ('Inlet Water Temperature = %.4f ',Twater_inlet)
```

```
            % rho = 6705; %density of composite in Kg/m3  %%FROM KEVIN
            rho_cyanate_ester = 1300 ; %Kg/m3
            rho_Cu = 8933; %Kg/m3 Earlier value 8940
            vol_fraction_Cu = 0.78;

            % Density of composite from volume fraction
            rho = (vol_fraction_Cu * rho_Cu) + ( (1-
vol_fraction_Cu)*rho_cyanate_ester );
            Cp_epoxy = 865;% Specific heat of epoxy in SI J/kg-K
            Cp_cu = 385; % Specific heat of Copper in SI J/kg-K
            Cp = (vol_fraction_Cu * Cp_cu) + ( (1-vol_fraction_Cu)*Cp_epoxy );
            rho_w = 1000; %density of water
            Cpw = 4200; %Specific heat of water

            % -----Geometry of tube --------
            ro = 0.005643326;% Outside radius in m
            ri = 0.003239/2; %inside radius in m
            %display ('Effective surface length L is :')
            L= (ro^2 - ri^2) / (2*ri) ;% Effective length calculated from Volume /
Surface Area
            %display ('Fourier number Fo is :')
            Fo = k/(rho*Cp) * t/L^2;
            vwater=7.13805/10^7; % Kinematic Viscosity of water
            Prwater=4.793; % Prandtl Number of water
            Re= (v)*(2*ri)/(vwater); %Reynolds number
            f = 1/((0.790*log(Re))-1.64)^2; % Darcy frictional factor
            Nu = ((f/8)*(Re-1000)*Prwater)/ (1+ (12.7*(f/8)^(1/2)*(Prwater^(2/3)-1)));
%               Nu=(0.027)*(Re^0.8)*(Prwater^0.4); %Nusselt number
            kwater=0.62495; %Thermal conductivity of water
            hwater= (Nu)*(kwater)/(2*ri); %Convective heat transfer coefficient of
water
%               hinverse=(1/hwater)+(3.5/hwater);
%               length_resistance=(k)*(3.5/hwater)
           hinverse=(1/hwater)+(0.089/k);%Inverse of the resistance term
            h=(1/hinverse);%Resistance term
            Bi= (h*L)/k; %Conductivity of composite.
%               sprintf('Length of heat resistance = %.6f',length_resistance)
            sprintf('Reynolds number = %.6f',Re)
            sprintf('Darcy friction factor = %.6f',f)
            sprintf('Nusselt number= %.6f',Nu)
            sprintf ('Biot Number = %.8f',Bi)
            mass_element_w = pi *(ri^2)* (length_of_tube/n) * rho_w ;
            mass_entire_composite = pi * (ro^2 - ri^2) *length_of_tube * rho ;
```

```
mass_each_element_composite = mass_entire_composite / n;

total_heat_lost_composite = mass_entire_composite * Cp * (Tcomposite -
Twater_inlet);
Tc(1:n)=Tcomposite; % intial temperature of composite in C
Tw(1:n) = Tcomposite;
Sum_of_DeltaT = 0 ;
count = 1;
temp=1;
DeltaT = 0;

%sprintf('Beginning of the first loop')
 for time=t:t:time_of_result

    for i=1:n

       Tcafter(i) = ((Tc(i)-Tw(i)) * exp(-Bi*Fo)) + Tw(i);
       Twafter(i) = Tw(i) + ( (ro^2-ri^2)*rho*Cp*( Tc(i)-
Tcafter(i)))/(ri^2*rho_w*Cpw);

    end

    T=Tcafter;
    m=n;
    a = kc /(rho * Cp); % thermal diffusivity of conductor in m^2/s
    Lx=length_of_tube/n;
    x = 0:(Lx/20):Lx;

    [p q] = size(x);
    s=1;
    while s<m-1;
    for j = 1:q
        add =  T(m-s-1);
        for r = 1:100
        Tx = -2/(r*pi)*(T(m-s+1)-T(m-s-
1))*cos(r*pi)*sin(r*pi*x(j)/Lx)+2/(r*pi)*((T(m-s)-T(m-s-1))*(1-cos(r*pi))+(T(m-s+1)-
T(m-s-1))*cos(r*pi))*exp(-a*(r^2*pi^2*time/Lx^2))*sin(r*pi*x(j)/Lx);
        add = add + Tx;
        end
        Tnew(j) = add;
    end

     A_graph = trapz(x,Tnew);
     A1_graph = trapz(x(1:11),Tnew(1:11));
```

```
  A3_graph = trapz(x(11:21),Tnew(11:21));
  A_half = T(m-s)*(Lx/2);
  A1 = A_half - A1_graph;
  A3 = A3_graph - A_half;
  Tm_2avg = (T(m-s-1)*Lx+A1)/Lx;
  Tm_1avg = A_graph/Lx;
  Tmavg = (T(m-s+1)*Lx-A3)/Lx;

  g(s,1)=Tm_2avg;
  g(s,2)=Tm_1avg;
  g(s,3)=Tmavg;

  T(m-s+1) = g(s,3);
  T(m-s)=g(s,2);
  T(m-s-1)=g(s,1);

  % "end of temp calculation for last 3 elements of the conductor"

% "beginning of temp. calculation of next 3 elements from the right"
  s=s+3;

end

Tlatest = T;


        % sprintf('end of the second loop',time)

       T_supply_element_Cu(count)=Tlatest(1*(n/n));
       T_mid500_element_Cu(count)=Tlatest(0.5*n);
       T_mid1000_element_Cu(count)=Tlatest(1*n);
       T_mid500_element_water(count)=Twafter(0.50*n);
       T_outlet_element_water(count)=Twafter(n);

       Tc = Tlatest;
       Twintermediate = Twafter;
       Twintermediate = Twintermediate( 1:(n-1) );
       Twnew=[Twater_inlet,Twintermediate];
       Tw=Twnew;

       time_steps(count)=time;
       T_bulk_Cu(count) = sum(Tcafter(0.980*n:n))/20 ;
       T_bulk_w(count) = sum(Twafter(0.980*n:20))/20;
       count = count + 1;
```

```
        end


    if  time_of_result - time > 0
       sprintf ('Temperature distribution was calculated at %.3f
seconds.\nTemperature distribution was requested at %.3f seconds.\nTo calculate at the
exact time, please increase the number of elements.',time,time_of_result)
    end

    time_steps_excel = time_steps(1:10:end);
      T_supply_element_Cu_excel=T_supply_element_Cu(1:10:end);
      T_mid500_element_Cu_excel=T_mid500_element_Cu(1:10:end);
      T_mid1000_element_Cu_excel=T_mid1000_element_Cu(1:10:end);
      T_mid500_element_water_excel=T_mid500_element_water(1:10:end);
      T_outlet_element_water_excel=T_outlet_element_water(1:10:end);
      T_bulk_Cu_excel=T_bulk_Cu(1:10:end);
      T_bulk_w_excel=T_bulk_w(1:10:end);


    % Make the second sheet active
    Sheets = Excel.ActiveWorkBook.Sheets;
    sheet_v = get(Sheets, 'Item', 1);
    invoke(sheet_v, 'Activate');

    % Get a handle to the active sheet
    Activesheet = Excel.Activesheet;

   % Put a MATLAB array into Excel
   ActivesheetRange = get(Activesheet,'Range','A2');
    set(ActivesheetRange, 'Value', 'time steps(s)');
    ActivesheetRange = get(Activesheet,'Range','A3:A65000');
    set(ActivesheetRange, 'Value', time_steps_excel(:));

   ActivesheetRange = get(Activesheet,'Range','B2');
    set(ActivesheetRange, 'Value', 'Supply Temp.(C)');
   ActivesheetRange = get(Activesheet,'Range','B3:B65000');
    set(ActivesheetRange, 'Value', T_supply_element_Cu_excel(:));

    ActivesheetRange = get(Activesheet,'Range','C2');
    set(ActivesheetRange, 'Value', '50% Cond Temp.(C)');
   ActivesheetRange = get(Activesheet,'Range','C3:C65000');
    set(ActivesheetRange, 'Value', T_mid500_element_Cu_excel(:));

    ActivesheetRange = get(Activesheet,'Range','D2');
```

```
 set(ActivesheetRange, 'Value', 'Return Temp.(C)');
ActivesheetRange = get(Activesheet,'Range','D3:D65000');
 set(ActivesheetRange, 'Value', T_mid1000_element_Cu_excel(:));

 ActivesheetRange = get(Activesheet,'Range','E2');
 set(ActivesheetRange, 'Value', 'Water 50%L Temp.(C)');
ActivesheetRange = get(Activesheet,'Range','E3:E65000');
 set(ActivesheetRange, 'Value', T_outlet_element_water_excel(:));

 ActivesheetRange = get(Activesheet,'Range','F2');
 set(ActivesheetRange, 'Value', 'Cu Temp. along length(C)');
ActivesheetRange = get(Activesheet,'Range','F3:F65000');
 set(ActivesheetRange, 'Value', Tcafter(:));

ActivesheetRange = get(Activesheet,'Range','G2');
 set(ActivesheetRange, 'Value', 'Water Temp. along length(C)');
ActivesheetRange = get(Activesheet,'Range','G3:G65000');
 set(ActivesheetRange, 'Value', Twafter(:));

 ActivesheetRange = get(Activesheet,'Range','H2');
 set(ActivesheetRange, 'Value', 'Cu bulk Temp. with time(C) ');
ActivesheetRange = get(Activesheet,'Range','H3:H65000');
 set(ActivesheetRange, 'Value', T_bulk_Cu_excel(:));

 ActivesheetRange = get(Activesheet,'Range','I2');
 set(ActivesheetRange, 'Value', 'Water bulk Temp. with time(C) ');
ActivesheetRange = get(Activesheet,'Range','I3:I65000');
 set(ActivesheetRange, 'Value', T_bulk_w_excel(:));

 ActivesheetRange = get(Activesheet,'Range','J2');
 set(ActivesheetRange, 'Value', 'Heat Loss)');
 ActivesheetRange = get(Activesheet,'Range','J3:J65000');

  ActivesheetRange = get(Activesheet,'Range','D1');
 set(ActivesheetRange, 'Value', 'RESULTS FOR For
Q=0.1g/min,Tw=9.91,Tc=60.18');


% Save the workbook
invoke(Workbook, 'SaveAs', '60C_0p1GPMp025');

total_time = cputime - start_time;
sprintf ('Actual running time of the model %.4f  minutes.',(total_time/60) )
```

VITA

Delight Mawunyo Owu was born on June 22, 1975 in Anfoega, Ghana. He was raised in Tema, a harbor city where he attended Star Primary and Junior Secondary School, a private school, for his elementary and middle school education. He continued to Presbyterian Secondary School, an all boys boarding school in the capital city, Accra, for his high school education. Upon completion, he moved to the garden city, Kumasi, to pursue a bachelor's in mechanical engineering at the University of Science and Technology, the only university in Ghana offering engineering. After four years of academic training, he graduated with honors in July, 1999. He worked with Ghana Aluminum Products, a corrugated roofing sheet manufacturer in Tema as a Maintenance Engineer, for a year. He moved to Tractor and Equipment, a caterpillar dealership in the capital city, Accra, for a Service Engineer position which he held for two years. He later moved to the United States for his graduate study. He started his graduate study in Mechanical Engineering at University of Tennessee, Knoxville, in the fall of 2007. He worked as a research assistant for Dr. Madhu Madhukar at the Magnet Development Laboratory on the Quasi-Poloidal Stellarator project, a United States government funded project which is being carried jointly by ORNL and the University of Tennessee. He will be graduating with his master's in Mechanical Engineering in May 2009.